NTNU – Trondheim
Norwegian University of
Science and Technology

Numerical modelling of Wood Microstructure

Trygve Stenrud Nilsen

Civil and Environmental Engineering (2 year)
Submission date: June 2015
Supervisor: Kjell A Malo, KT

Norwegian University of Science and Technology
Department of Structural Engineering

Preface

This thesis is the finishing project of a 2-year master degree in civil and environmental engineering at the Norwegian University of Science and Technology (NTNU). The thesis was written during the spring of 2015 under the department of structural engineering.

The main goal of this thesis is to investigate the possibilities that lie in numerical modelling of the microstructure of wood for structural engineering. It consists of a theoretical introduction and numerical tests carried out in the commercially available finite element program ABAQUS FEA.

I would like to thank my supervisor Kjell Arne Malo for his help during the spring. Without him to guide me in the right directions when I was stuck, I would not have come as far.

Trondheim, June 2015

Trygve Stenrud Nilsen

Abstract

The behaviour of wood is hard to predict due to the complex structure of the material. Wood consists of cells (fibres) arranged in an intricate pattern, and the behaviour of the material is a result of the behaviour of the cells and the cell arrangement. In this thesis, a new approach to numerical modelling of wood has been investigated, using the commercially available finite element program ABAQUS FEA. Instead of modelling wood with macroscopic properties and geometry, the cellular microstructure has been modelled. The cellular structure was modelled using shell elements, assigned the microscopic material properties of the cell walls and loaded with transverse compression.

An important point of the modelling process was to capture known physical effects that come into play in wood subjected to transverse compression. Especially the hammock effect and the effect of load distribution to the untouched areas of wood for increased stiffness and capacity needed to be included.

Due to the highly non-linear nature of the problem (buckling, material non-linearity and self-contact), an explicit dynamic formulation was used to analyse the problem. Modelling quasi-static problems with explicit dynamics requires the solution to be carefully controlled to ensure that the dynamic forces are insignificant so that the solution found is the quasi-static one. One way ensuring that dynamic forces are small compared to the static forces, is to look at the energy balance. If the kinetic energy and energy dissipated due to damping is significantly lower than the strain energy, the dynamic forces can be assumed insignificant.

In the results, load-deformation curves produced from the numerical simulations was presented and compared with load-deformation curves from previous lab experiments. The load-deformation curve of the numerical model resembled to some degree those of lab tests. Initially, the relationship between load and deformation was linear, and the linearity transitioned to a strain-hardening phase where the deformation increased and the load was close to constant. The hammock effect and load-distribution effect was seen clearly in the results, where the models with untouched wood on the side of the loaded area had higher stiffness and strength.

The results were plagued by a numerical instability phenomenon that occurred when the deformation was so large that many cells were completely caved in. This instability manifested itself through the load-deformation curve, which started out very smooth, but transitioned into a noisy and “spiky” curve towards the end. Numerical damping was applied to the model, which is seen in the energy balance. The energy dissipated due to numerical damping grew from a few percent to roughly 15% of the strain energy.

Design of small wood components, such as joints, requires a good material model in order to predict capacity and failure modes accurately. If developed further, microstructure modelling of wood can be a very helpful tool to predict the behaviour and capacity of wood components.

Samandrag

Materialoppførselen til tre er vanskeleg å forutsjå grunna den komplekse oppbygginga til materialet. Tre er bygd opp av celler som ligg tett i tett i eit mønster, og materialeigenskapane avheng av eigenskapa til cellene og cellemønsteret. I denne oppgåva har ei ny tilnærming til numerisk modellering av tre blitt prøvd ut I elementmetodeprogrammet ABAQUS FEA. I staden for å modellere tre med sine makroskopiske eigenskapar og geometri har mikrostrukturen av cellene vore modellert. Cellestrukturen vert modellert som eit regulært sekskantmønster, tildelt dei mikroskopiske materialeigenskapa til ein cellevegg og lasta på med trykk normalt på fiberretninga.

Eit viktig poeng med mikromodelleringa var å fange kjente effektar som verkar på tre under tverrtrykk. Hengekøye-effekten og lastfordeling under det pålasta arealet kan auke stivleiken og styrka, og innverknaden av desse effektane blei undersøkt i resultatet frå dei numeriske simuleringane.

Tre belasta med trykk på tvers av fiberretning er i høgaste grad eit ikkje-lineært problem på mikroskala nivå. Treceller blir samanklemt, celleveggar knekk saman og får sjølvkontakt i tillegg til at materialet i celleveggene ikkje oppfører seg lineært ved store spenningar. For å unngå konvergensproblema slike ikkje-lineæritetar medfører, vert det brukt eksplisitt dynamikk for å køyre analysa. Når ein køyrer kvasi-statiske analyser med ei dynamisk formulering krevjast det at ein kontrollerer at dei dynamiske kreftane er små nok til å kunne ignorerast. Ein måte å gjere dette på er å sjå på energibalansa. Den kinetiske energien og dempningsenergien må være mykje lågare enn tøyningsenergien.

Mange laboratorieforsøk på tre utsatt for trykk normalt på fiberretning er utført av andre, så det er ikkje vore utført noko lab-forsøk i denne oppgåva. Last-deformasjonskurver frå dei numeriske forsøka vert samanlikna med data frå lab-forsøk frå ei anna masteroppgåve. Resultata viste noko samsvar med lab forsøka. I byrjinga av pålastinga var forholdet mellom kraft og forskyving lineært, som gjekk over til eit flyteplatå der forskyvinga auka utan at krafta auka. Hengekøyeeffekten og lastfordelingseffekten kom klart fram i resultatet, der modellane med urørt tre på kvar side av lasta hadde høgare stivleik og styrke.

Resultata var plaga av ein form for numerisk instabilitet som kom fram når deformasjonen var så stor at fleire celler hadde kollapsa. Denne instabiliteten viste seg i last-forskyvningskurva, som i byrjinga var ei glatt kurve, men som var prega av støy mot slutten. Numerisk demping vert automatisk påført av ABAQUS til å dempe denne støyen, noko som kan sjåast i energibalansa. Energien som gjekk med til demping vaks frå eit par prosent til nærmare 15% prosent av tøyningsenergien.

Med meir utvikling så kan mikrostrukturmodellering av tre vera eit godt reiskap til å forutsjå oppførselen og kapasiteten til tre. Spesielt ved design av forbindingar er ein avhengig av ein god materialmodell som beskriv ikkje-lineæritetar for å kunne forutsjå kapasitet og brotmoder.

Table of contents

1 Introduction

Wood is one of the oldest and most used materials known. From a simple log lying over a creek acting as a footbridge to large multi-storey timber buildings, wood is usable for a wide range of structures. In recent years, large bridges and tall timber buildings are getting increased attention. When we push the limits on how large timber structures we build, increased difficulties arise with the design and building process. With increased size comes larger demands towards safety and durability, and a need for more accurate tools to predict the behaviour of the structure rises, both in the construction phase and the finished structure. One has to verify that the structure is safe and that the demands set by building codes and regulations are satisfied.

One way to show that a structure is satisfactory is to create a prototype and test this. Creating a prototype for every structure we build would be very expensive and impractical, so other means of predicting structural behaviour is required. Computer simulations is a good way to predict how a structure will behave. Instead of creating and testing prototypes, we can create a digital model and test this with different analysis techniques.

The most common analysis technique in structural engineering is the finite element method (FEM). In FEM, a structure is divided into several small parts (elements), where each element's behaviour is "known", and the behaviour of the system is a result of the behaviour of each element. In this thesis, the numerical simulations are carried out on the commercially available software ABAQUS FEA.

Computer simulations of structural behaviour can be split into two parts, global and local analysis. Global behaviour refers to the response of an entire structure subjected to various loads (wind, snow, dead load etc.). The global analysis shows how forces transmit through a structure, e.g. how snow load on the roof transfers through a building into the ground. In the local analysis, we look at the response of a single structural element, e.g. finding the capacity of a column-to-beam connection.

If we want to analyse a timber connection, we need to know how wood behaves when stressed close to failure. The mechanical behaviour of wood, especially close to failure, is hard to describe since wood is a very complex material. Each block of wood is slightly different from another wood block, and the mechanical behaviour is dependent on the direction of loading and moisture content.

When we look at a wooden block with the naked eye, we see a continuous material (a continuum). If we look at a wooden block under the microscope, we see cells (fibres) tied closely together in an intricate pattern called the cell structure. In this thesis, a new approach to numerical modelling of wood has been investigated. By modelling the wood as a

collection of cells rather than a continuum, one can possibly get a more accurate prediction of the material behaviour.

The thesis consists of a theoretical introduction to wood microstructure and the analysis techniques used, a chapter describing the modelling process in ABAQUS in addition to results and discussion.

2 Theory

2.1 The structure of wood

From a structural point of view, the purpose of a tree is to give sunlight to its leaves. In order to give its leaves sunlight, the tree has to place the leaves up in the air to avoid shadows from nearby objects. The tree has to grow taller to give its leaves better light, and when it gets taller the loads on the stem increases, due to increased self-weight and wind loads. In order to deal with the increasing loads the tree has to become thicker, which further increases the load. The balance between strength and loading needs to be optimal. In reality, trees are highly efficient in doing this. The material has to be light to reduce the self-weight, but strong enough to take the external forces due to wind and snow, and it need to be able to damp out vibration caused from dynamic loads. In addition, the tree has to be able to transport water and nutrients.

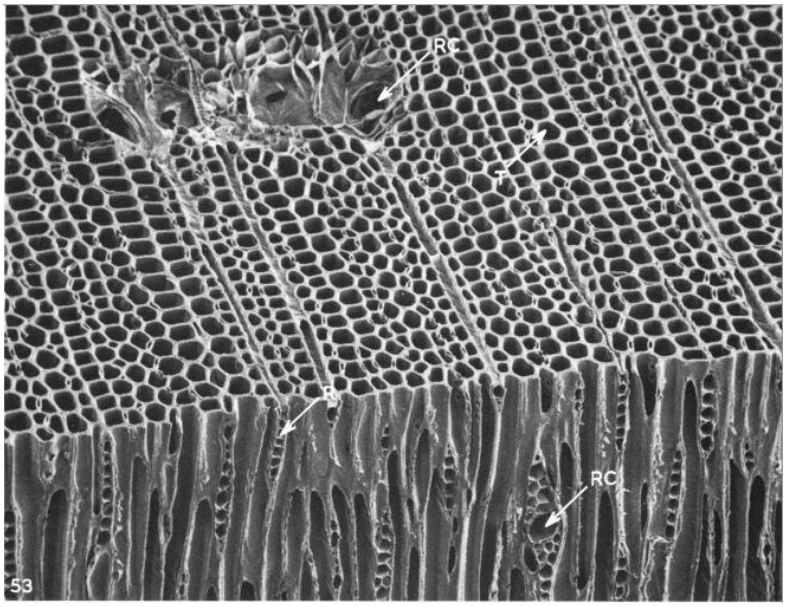

Figure 1: cellular structure of a softwood [1]

One way to make something light and stiff is to build it in a truss-like way, and this is also how trees are built. The inner part of the tree, the xylem, which carries the loads, are made up of polygonally shaped hollow cells arranged in a pattern, see Figure 1 [1]. When the tree grows in the width direction, new cells are created outside the existing cells [2]. In the spring, the cells grow quickly causing large cells with plenty of open space, called earlywood [3]. Through the summer and autumn, the growth rate slows down and the cells become denser with less open space, called latewood [3, 4]. This causes the cross-section to have alternating light and dark rings with earlywood and latewood, also known as annual rings [1]. The fibre-like cells spanning the longitudinal direction and the annual rings is what gives wood its unique directionally dependent material properties [3].

2.2 Structure of cells

In softwoods, the xylem consists of cells (fibres) which look like small tubes, with a diameter of 20-50 µm in diameter and 2-4 mm in length [5] [6].

The cell walls consist of different layers, each with unique behaviour and purpose. Most of these layers are fiber-reinforced polymer laminates, where microfibrils made of cellulose act as reinforcement and hemicellulose and lignin makes up the matrix that binds everything together [5, 7]. The thickness and microfibril arrangement and thus the mechanical properties varies from layer to layer. These layers are sorted into three different categories, the middle lamella, the primary wall and the secondary wall. The secondary wall can be subdivided into three layers; S1, S2 and S3 [6].

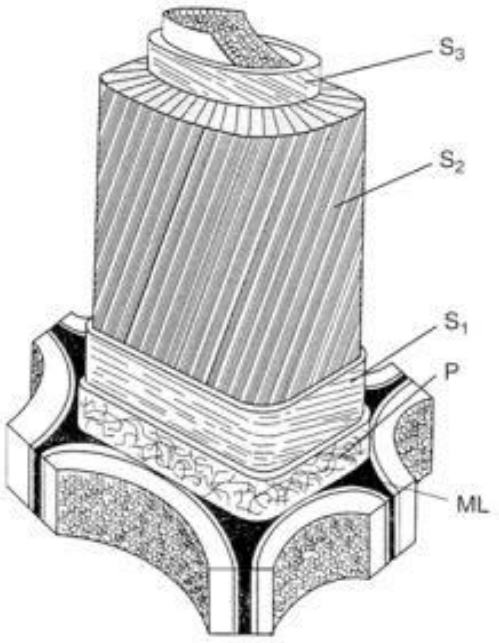

Figure 2: The structure of a single cell [8]

The thickness of the cell walls varies within the xylem. Latewood cells have thicker walls than earlywood cells. Exact cell wall thicknesses are hard to come by, but Booker and Sell estimates the thickness of the dominating layer (S2-layer) to be 1-5 µm [8]. The S2-layer makes up roughly 75% of the cell walls [3], thus the cell walls can be estimated to be 2-7 µm.

The mechanical properties of the cell walls are the same for all species of trees. Different properties of different species come from different *cell structure geometry.* The reason for this is that the layer which the trees gets most of its mechanical properties, the S2 layer, varies little between different tree species [7].

2.2.1 Secondary wall

The secondary wall makes up about 75% of the cell wall thickness and is where wood gets most of its stiffness properties [3]. As mentioned before, the secondary wall consists of three layers, the outer layer S1, the middle layer S2 and the inner layer S3. Each of these layers are fiber-reinforced with microfibrils, and the microfibril angle (MFA) is different in each layer [3].

The S1 and S3 layer have relatively large MFA (between 50-90 degrees) and are similar in thickness. Together they make up about 15% of the secondary wall. The S2 layer is the thickest of the three and makes up about 85% of the secondary wall, and has relatively small MFA (10-30 degrees). The thickness and MFA of the S2 layer causes this layer to have a great effect on the cell wall properties and the mechanical properties of the tree. [7] [8]

The microfibrils in the S1 and S3 layer are roughly perpendicular to the fibres in the S2 layer. Between the S1, S2 and S3 layer lies transition layers S12 and S23 that ensures a smooth transition between the layers. It is convenient to combine the S12 and S1 layers and the S23 and S3 layers when describing the cell wall properties. [8]

The S1 layer

The outermost layer encloses the S2 layer and has microfibrils spiralling around the wall in a helix. The microfibril angle varies from 45° to 90°. Its purpose is to prevent the S2 layer from increasing in diameter when compressed, which also limits the shear forces in the middle lamella. [8]

The S2 layer

The middle layer is the thickest and takes up most of the longitudinal forces in the wood. The microfibrils are oriented nearly parallel to the fibre direction, with the MFA ranging from 5° to 30°. Fiber-reinforced laminates are stiffest when loaded in the fiber-direction, so it is beneficial to have small MFA in this layer. Ideally, the MFA should be zero, which would utilize the microfibrils the most. A slight angle makes it harder for cracks to propagate through the cells, which is why the microfibrils are angled the way they are. In addition, with slightly angled microfibrils, the cell will rotate when subjected to compression or tension. This rotation is opposite in the neighbouring cells, which creates friction forces in the middle lamella. The friction forces dissipate some energy, and the slightly angled microfibrils thus creates a damping mechanism in the xylem. This damping mechanism makes the tree better at resisting dynamic forces. [8]

The S3 layer

Within the innermost layer there is an empty space called the lumen. The lumen transports water up to the leaves, and to transport water against the gravity one needs pressure. The main task of the S3 layer is to prevent the cells from buckling under the hydrostatic tension forces in the lumen. The microfibrils are angled from 30* to the 60*, depending on where in the layer we look. The S3 layer also contributes to preventing transwall fractures. [8]

2.2.2 Primary wall and middle lamella

The middle lamella and the primary wall's main task is to join cells together and resist delamination between the secondary walls on either side. In this context, the primary wall and middle lamella work together so closely that they are considered as one. From now on, they are referred to as the compound middle lamella (CML). The CML consists mainly of lignin and is therefore relatively soft. The main forces this layer takes up are the friction forces associated with the damping mechanism mentioned 1.2.1. [8]

2.3 Mechanical properties of wood

Due to its unique cell structure, wood as a material is light, stiff and strong. The strength to weight ratio is similar to that of structural steel [5]. The stiffness and strength vary greatly with the direction of the material [6]. The mechanical properties can be described on different anatomical scales, see figure 3. The most common is to describe the properties on the macro scale (clear wood), which obviously is most useful for actual engineering application [3]. The disadvantage in describing mechanical properties of wood on the macro scale is the difficulties that lie in predicting the non-linear behaviour.

Figure 3: Anatomical scales of wood

In order to understand the non-linear behaviour of wood, one has to look at the cellular structure. A brief description of mechanical properties of wood in the macro and micro scale is presented in chapter 1.3.1-1.3.3.

2.3.1 Macro scale (clear wood)

Linear elastic orthotropic behaviour

Wood can be assumed linear elastic for moderate loads and short term loading [3]. If material properties vary with the direction of a material, the material defined as is anisotropic. If orthogonal planes of material symmetry can be found, the material is orthotropic. Due to the unique cell structure in wood, three planes of material symmetry exist, which makes wood an orthotropic material. The three planes are the radial, tangential and longitudinal plane [6]. The strength and stiffness properties of wood vary greatly from the longitudinal direction to the tangential and radial direction. In table 1, typical values for structural wood is presented. The values themselves are not of great interest since values vary from literature to literature. Note the great difference in the longitudinal and transverse directions.

ρ	E_{LL}	E_{RR}	E_{TT}	G_{LR}	G_{LT}	G_{RT}	υ_{LR}	υ_{LT}	υ_{RT}
350 kg/m^3	10300 MPa	690 MPa	410 MPa	620 MPa	620 MPa	50 MPa	0.76	-	0.49

Table 1 Example of macroscopic material properties of wood [6]

Figure 4: cross section of a tree. Taken from Wikipedia [9].

If a wood block is cut close to the pith (the centre line running longitudinally through the stem, see Figure 4), a cylindrical coordinate system can be used to describe the material properties, since the annual rings curvature close to the pith is large. Likewise, if the wood block is cut further away from the pith, the annual rings appear almost straight and one can use a rectangular coordinate system. Hooke's law for wood in three dimensions (longitudinal, radial and tangential) is defined as [3]:

$$\begin{Bmatrix} \varepsilon_{LL} \\ \varepsilon_{RR} \\ \varepsilon_{TT} \\ \gamma_{LR} \\ \gamma_{LT} \\ \gamma_{RT} \end{Bmatrix} = \begin{bmatrix} \frac{1}{E_L} & \frac{-\upsilon_{RL}}{E_R} & \frac{-\upsilon_{TL}}{E_T} & 0 & 0 & 0 \\ \frac{-\upsilon_{LR}}{E_L} & \frac{1}{E_R} & \frac{-\upsilon_{TR}}{E_T} & 0 & 0 & 0 \\ \frac{-\upsilon_{LT}}{E_L} & \frac{-\upsilon_{RT}}{E_R} & \frac{1}{E_T} & 0 & 0 & 0 \\ 0 & 0 & 0 & \frac{1}{G_{LR}} & 0 & 0 \\ 0 & 0 & 0 & 0 & \frac{1}{G_{LT}} & 0 \\ 0 & 0 & 0 & 0 & 0 & G_{RT} \end{bmatrix} \begin{Bmatrix} \sigma_{LL} \\ \sigma_{RR} \\ \sigma_{TT} \\ \tau_{LR} \\ \tau_{LT} \\ \tau_{RT} \end{Bmatrix} \textbf{(Equation 1)}$$

For practical purposes, the radial and tangential direction are often combined, reducing the three dimensional material description into two directions: the longitudinal and transverse direction. Hooke's law (eq. 1) reduces to [3]:

$$\begin{Bmatrix} \varepsilon_{11} \\ \varepsilon_{22} \\ \gamma_{12} \end{Bmatrix} = \begin{bmatrix} \frac{1}{E_1} & \frac{-\upsilon_{21}}{E_2} & 0 \\ \frac{-\upsilon_{12}}{E_1} & \frac{1}{E_2} & 0 \\ 0 & 0 & \frac{1}{G_{12}} \end{bmatrix} \begin{Bmatrix} \sigma_{11} \\ \sigma_{22} \\ \tau_{12} \end{Bmatrix} \textbf{Equation 2}$$

In addition to the direction of the material, the mechanical properties depend on density, duration of loading (creep) and moisture [3].

Non-linear behaviour and failure

The mechanical properties of wood in the elastic range are relatively easily described. Difficulties arise when describing the nonlinear mechanical properties. Wood is characterized as brittle in tension and shear and ductile in compression [3]. Plasticity models developed for metals can in some cases be used for wood, but no plasticity model exists that can generally describe wood.

One example of a plasticity model that is usable for wood is the crushable foam plasticity model. However, the crushable foam model requires the elastic properties to be defined as isotropic, making it unsuitable for wood in general. [10]

2.3.2 Micro scale

Cell wall

As mentioned in chapter 1.2, the cell walls consist of fiber-reinforced polymer laminates. Therefore, the mechanical behaviour of cell walls is similar to that of fiber-reinforced polymers. Typical behaviour for polymers is visco-elasticity and temperature dependent properties. When stressed, a polymer like a cell wall will get a certain strain. The strain is dependent on the loading (elasticity) and the duration of loading (visco-elasticity). This visco-elasticity in the cell wall is the reason wood will get a creep effect on long term loading. [7]

Kettunen [7] suggests that the mechanical properties of cell walls in moist wood are as follows. Note that the cell walls are roughly three times stronger and stiffer in the axial direction than the transverse direction

	Axial	Transverse
Density [kg/m3]	1500	1500
Young's modulus [MPa]	35000	10000
Yield strength [MPa]	150	50

Table 2: Mechanical properties of the cell walls

Binding the cells together lies the compound middle lamella made out of lignin. The mechanical properties of lignin can according to Smith et al. be described by the isotropic stiffness matrix [3]:

$$D_{Lignin} = \begin{bmatrix} 4 & 2 & 2 & 0 & 0 & 0 \\ 2 & 4 & 2 & 0 & 0 & 0 \\ 2 & 2 & 4 & 0 & 0 & 0 \\ 0 & 0 & 0 & 1 & 0 & 0 \\ 0 & 0 & 0 & 0 & 1 & 0 \\ 0 & 0 & 0 & 0 & 0 & 1 \end{bmatrix} c_L(m) \text{ GPa}$$

Eq 3

Where $c_L = \frac{1+2(1-m)}{1+a}$ is a factor that takes moisture contentment into account.

Here, *m* is the moisture content and *a* is an "area compensation factor" which is set to 1. Assuming 20% moisture, the C_L factor becomes 1.3. The Poisson's ratio suggested by Bergander is 0.3 [11].

Taking the E-modulus from Eq 3 and the Poisson's ratio from Bergander, lignin can be simplyfied as an isotropic material, see table 3.

E-modulus (GPa)	4x1.3 = 5.2
Poisson ratio	0.3

Table 3: Mechanical properties of lignin

Cell structure

The cell structure of wood is for simplicity idealized as a regular honeycomb-type pattern. This is not the case in a real tree since not all cells are hexagonal or equally sized, but for practical purposes, the irregularities in the cell structure is for now neglected [7].

When compressed transversely, a honeycomb pattern will first deform elastically. Following the elastic deformation, cell walls will begin to buckle, causing cell layers to cave in on themselves. When cells collapse, the inner walls will come in self-contact, causing an increase in stiffness [7].

The load-displacement curve will then begin linearly, followed by a strain-hardening region where strain increases with little increase in stress caused by (caused by cell wall buckling). After the strain-hardening, a further increase in stiffness can sometimes be noticed, which is caused by self-contact in the cells [7].

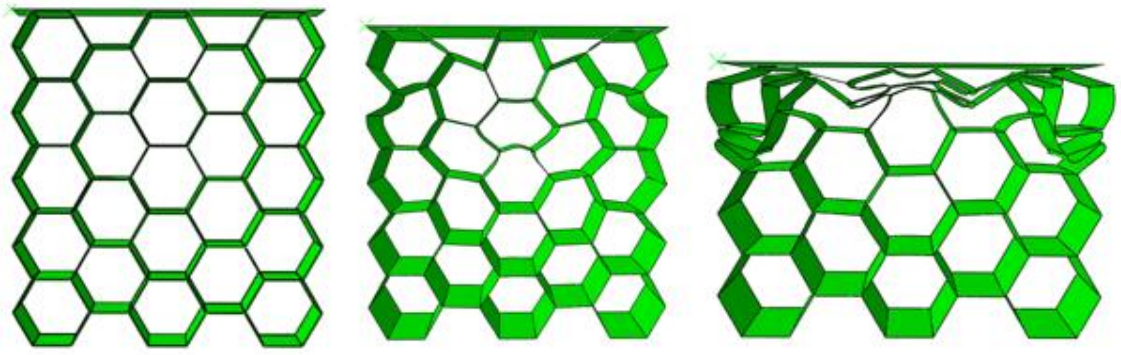

Figure 5: A honeycomb structure that goes from undeformed (left), slightly deformed with small bending and buckling of cell walls (middle) and severe crushing with self-contact (right). (From ABAQUS model)

The real cell structure of wood is highly irregular, with cells varying greatly in size and thickness from earlywood to latewood. In an irregular honeycomb “mesh”, the weakest walls are the first to collapse, which is why it is difficult to separate elastic and plastic behaviour. The weak walls might have undergone severe irreversible deformation, while stronger walls are still in the elastic range. [7]

The cell structure is also the reason for wood’s anisotropic behaviour. Just as a single cell behaves completely differently when loaded transversely and the longitudinal direction, the cell structure does. In the macro scale, the transverse direction is usually a combination of radial and tangential direction, dependent on how the wood is oriented [7].

In summary, the macroscopic behaviour of wood is the result of both cell wall behaviour and cell structure behaviour

2.3.3 Wood in transverse compression

The compression capacity of a wood specimen loaded perpendicular to the grain depends mainly on the compression strength of the material and two main effects. First, if there is untouched wood on either side of the loaded area, the forces will spread out over a larger "effective" area, thus increasing the capacity.

Secondly, given that there is untouched wood on either side of the loaded area, the so-called hammock effect increase the capacity further. The hammock effect is the additional strength that comes from the fibres acting as ropes or cables in tension holding up the deformed area from the sides (see Figure 6).

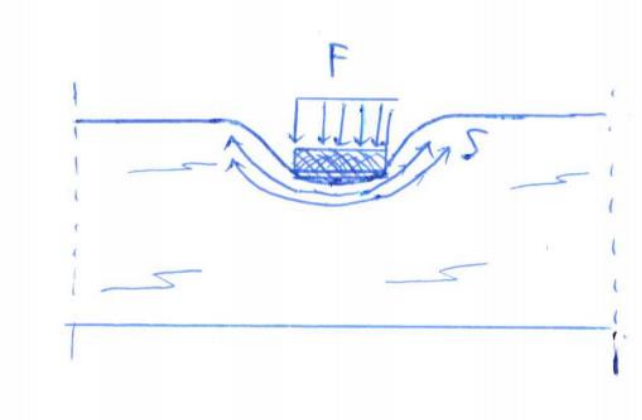

Figure 6: The hammock effect

Load-deformation curve

Below, two load-deformation curves are presented from the master thesis of Joakim Troller [12]. They are the result of compression tests of timber sills with varying height and constant area. The dimensions are 89x90 mm, with height varying from 30 mm to 90 mm.

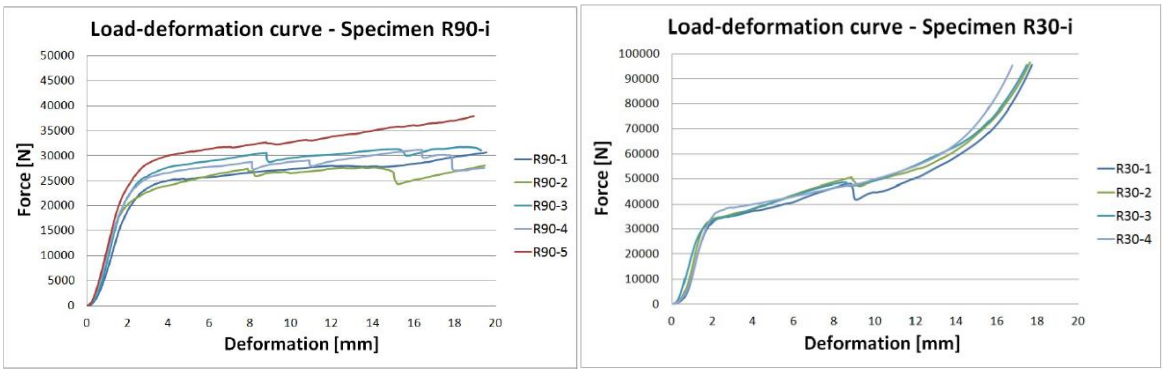

Figure 7: Load-deformation curves from Troller. The height of the test specimens is 90mm on the left graph and 30mm on the right.

In the load-deformation curves from specimen R90-I, which is the specimen with height 90 mm, the elastic part and strain hardening part is easily seen. When the height is reduced to 30 mm, we can also see the increase in stiffness caused by cell self-contact.

Eurocode 5 capacity model:

In Eurocode 5, the compression capacity perpendicular to the grain is calculated as [13]:

$$\sigma_{c,90,d} = \frac{F_{c,90,d}}{A_{ef}} \leq k_{c,90} f_{c,90,d} \quad \textbf{Eq. 4}$$

Where

$\sigma_{c,90,d}$ is the design compressive stress in the effective area

$F_{c,90,d}$ is the design compressive force perpendicular to the grain

A_{ef} is the effective area

$f_{c,90,d}$ is the design compressive strength of the material

$k_{c,90}$ is a factor that takes hammock effect into account

If there is untouched timber on either side of the loaded area, the area can be increased by 30 mm in each direction, but not more than a, l or $l_1/2$, see Figure 8.

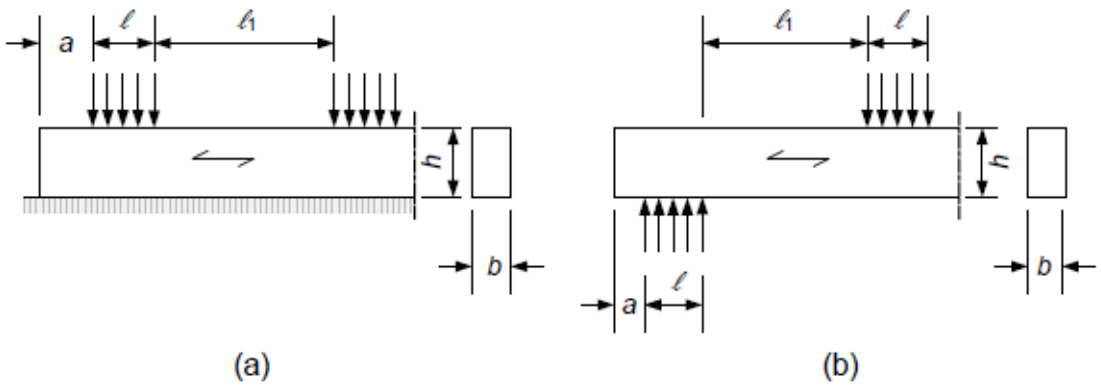

Figure 8: Effect of untouched wood from Eurocode 5 [13]

2.4 Finite Element Analysis (FEA)

Finite element analysis is a numerical method for solving field problems described by a set of partial differential equations. The method takes a structure and subdivides it into a system of smaller elements (finite elements), called a mesh. The stiffness relations of each element then found by *assuming* a displacement field within the element. Then the stiffness relations of each element are assembled to form the system stiffness relation. When this is done, the once complex system is broken down into a set of algebraic equations, that the computer solves and produces the desired variables (displacements, strains, temperatures etc.). [14]

FEA can be used to solve both static and dynamic problems, which can be linear or nonlinear. In this thesis, the finite element method is applied to model the crushing of a wood block, which is a highly non-linear problem.

2.4.1 ABAQUS

ABAQUS FEA is a general purpose finite element program. It consists of several parts, aimed to solve different kinds of problems.

1. Abaqus CAE (Complete Abaqus Environment) is a software used for modelling mechanical components and visualizing the results
2. Abaqus/Standard is a finite element analyser that uses an implicit integration scheme
3. Abaqus/Explicit is a finite element analyser that uses an explicit integration scheme

In addition, there is Abaqus/CFD, which solves fluid dynamic problems.

In this thesis, Abaqus CAE has been used for creating the model and viewing the results and Abaqus/Explicit has been used to solve the problem.

2.4.2 Quasi-Static simulations using explicit dynamics

When working with severely nonlinear problems, convergence difficulties can make it difficult to use a static implicit analysis. One example is to look at column in compression close to buckling. When buckling occurs, the compressive strain is “instantly” converted to bending strain and the system stiffness decreases radically. In such a case, static equilibrium is hard to find, since the system stiffness is reduced drastically over a very short time span. Static equilibrium is in general hard to establish in severely nonlinear analysis with buckling, material hardening and contact, since the load-deformation curve is not smooth. [15]

Another approach is to analyse it using explicit dynamic techniques. Instead of true static equilibrium in each increment, dynamic equilibrium is established, which includes inertia and damping forces. Such sudden movements like buckling is then retarded by inertia forces, making equilibrium easy to establish. Using an explicit dynamic formulation for quasi-static simulations introduces other problems that needs to be taken into account. The main difficulty with quasi-static simulations using explicit dynamics is to know if the solution found is close to the true static solution. [10]

If the loading is applied too quickly, inertia forces will dominate. If inertia forces are large compared to the stiffness forces, the solution found is not the quasi-static solution. One way of avoiding this is to apply the loading at the same speed as in "reality". Quasi-static loads in reality are very slowly applied, perhaps over the span of several minutes. If one were to use this "real" time span in an explicit analysis, millions of increments would be required, making the analysis very expensive in terms of CPU time. There are techniques to decrease the CPU cost (mass scaling and increasing load rates), but they must be used with care to ensure that the inertia forces are insignificant. [16]

2.4.2.1 Stability of solution

An explicit dynamic analysis is only conditionally stable. In order for the analysis to be stable, the time increments has to be smaller than the *largest stable time increment*, which for an undamped system is [10]:

$$\Delta t \leq \frac{2}{\omega_{\max}} \quad \textbf{Eq. 5}$$

Where $\omega_{\max}$ is the highest eigenmode of the system.

To damp out high frequency vibration ("ringing"), ABAQUS introduces numerical damping. The stability limit of a damped system is [10]:

$$\Delta t \leq \frac{2}{\omega_{\max}}(\sqrt{1+\xi^2} - \xi) \quad \textbf{Eq. 6}$$

A good estimate for the largest stable time increment is the time a wave uses to propagate through an element [10]:

$$\Delta \mathrm{t} = \left(\frac{L^e}{c_d} \right) \quad \textbf{Eq. 7}$$

Where L^e is the characteristic element length of the smallest element and c_d is the dilatational wave speed in the material. The wave speed in a linear elastic material with zero Poisson's ratio is [10]:

$$c_d = \sqrt{\frac{E}{\rho}} \quad \textbf{Eq. 8}$$

Where E is the young's modulus and ρ is the density of the material.

2.4.2.2 Techniques to reduce CPU cost

If the largest stable time increment is very small, a large amount of increments has to be calculated to finish the analysis, which will increase the computational time. In order to minimize computational time, it is desirable to have as few increments as possible. Measures to reduce the number of increments can be either to reduce the time span of the simulation or to increase the stable increment size. The stable increment size can be increased according to equation 7 by either increasing the size of the elements (L^e) or decreasing the dilation wave speed (c_d). [16]

The goal of these measures is to make the analysis as efficient as possible while still keeping the dynamic forces to an insignificant level.

Increasing element size

Increasing the element size increases the time a wave uses to propagate through the element, which increases the stability limit and allows larger time increments to be used. In addition, increasing element size decreases the number of elements and degrees of freedom in the model, which naturally makes the problem smaller and faster to solve.

Decreasing dilation wave speed

The wave speed can be decreased by either decreasing the E-modulus or increasing the mass. In quasi-static simulations, accurate estimates of the stiffness forces are desired, so changing the E-modulus is not recommended. Scaling the mass instead, is a good way to speed up an analysis [16]. If we increase the mass by a factor of x^2, we reduce the wave speed by a factor of x, and thus increase the stable time increment by a factor of x (see eq. 7 and 8). For example, if we scale the mass of the entire model by 4, the stable time increment doubles and the analysis time is halved. If inertia forces are still small enough to be neglected, we have a more efficient model.

Increasing loading rates

By shortening the time span of the simulation, fewer increments have to be made to complete the analysis, thus speeding up the analysis. Increasing the load rate would result in artificially high strain rates in the material. If materials were strain-rate dependent, changing the loading rates would change the response. Then, mass scaling should be used instead. [10]

2.4.2.2 Energy balance

If a model is producing unrealistic results, one way to uncover this is to check the energy balance. In this case, explicit dynamics are applied to model a quasi-static problem. The dynamic forces (inertia and damping forces) should therefore be negligible compared to the static forces ("stiffness forces"). If the internal energy is significantly larger than the kinetic energy and the damping energy, it is safe to assume that the static forces are dominating [10].

With explicit dynamics, numerical instability is also a factor that can drastically change results. Numerical instability can be uncovered by looking at the total energy balance. Energy balance is calculated according to equation 9 [10]. This energy balance should be constant or close to constant throughout the analysis.

$$E_{TOTAL} = E_{Kinetic} + E_{Internal} + E_{VD} - W_{External} \quad \textbf{Equation 9}$$

2.4.3 Progressive damage and failure

When making numerical models predicting the collapse of a structure, a way of describing material failure is required. Because of the strong directionally dependent properties of wood, it is hard to find a failure criterion that accurately predict the failure modes. Failure theories for wood needs to take into account the orthotropy of wood, direction of loading (tension vs compression) and the interaction of stresses. Commonly used theories are the Hankinson formula, Norris criterion and Tsai-Wu criterion [6].

The scope of this thesis is to focus on the cellular microstructure of wood, and the layers in the cell walls are in essence fibre-reinforced composites. The damage model developed by Hashin [17] to describe failure in fibre-reinforced composites should therefore be suitable to describe the failure modes and non-linearity of the cell walls.

Hashin damage

Limitations: Hashin damage criteria can only be used with linear elastic material and with plane stress elements. [10]

Four different failure modes are included in the Hashin damage criteria [17]:

Fiber tension: $$F_f{}^t = (\frac{\sigma_{11}}{X^T})^2 + \alpha(\frac{\hat{\tau}_{12}}{S^L})^2$$

Fiber compression: $$F_f{}^c = (\frac{\sigma_{11}}{X^C})^2$$

Matrix tension: $$F_m{}^t = (\frac{\sigma_{22}}{Y^T})^2 + (\frac{\hat{\tau}_{12}}{S^L})^2$$

Matrix compression: $$F_m{}^c = (\frac{\sigma_{22}}{2S^T})^2 + [(\frac{Y^C}{2S^T})^2 - 1]\frac{\sigma_{22}}{Y^C} + (\frac{\hat{\tau}_{12}}{S^L})^2$$

Where X^T and X^C is the longitudinal tension and compression strength of the composite, Y^T and Y^C is the transverse tension and compression strength and S^L and S^T is the longitudinal and transverse shear strength. $\sigma_{11}, \sigma_{22}, \hat{\tau}_{12}$ denotes the effective stresses in each direction, which are computed from the damage operator **M** and true stress tensor **σ**, see eq. 10. [10]

$$\sigma = M\sigma \quad \textbf{Eq. 10}$$

The damage operator is a 3x3 matrix that contains the damage variables for the fiber direction, transverse direction (matrix) and shear direction.

$$M = \begin{pmatrix} \frac{1}{(1-d_f)} & 0 & 0 \\ 0 & \frac{1}{(1-d_m)} & 0 \\ 0 & 0 & \frac{1}{(1-d_s)} \end{pmatrix} \quad \textbf{Eq. 11}$$

The constitutive law is assumed linear between stresses and strains. H_0 contains the elasticity parameters of the undamaged material [17]:

$$\varepsilon = H_0 \sigma, \qquad \text{where} \quad H_0 = \begin{pmatrix} \frac{1}{E_{11}} & -\frac{\upsilon_{21}}{E_{11}} & 0 \\ -\frac{\upsilon_{12}}{E_{22}} & \frac{1}{E_{22}} & 0 \\ 0 & 0 & \frac{1}{G} \end{pmatrix} \quad \textbf{Eq. 12}$$

Equation 10 and 12 combined gives

$$\varepsilon = H_0 \sigma = H_0 M \sigma = H \sigma \quad \textbf{Eq. 13}$$

$$\text{Where } H = \begin{pmatrix} \frac{1}{(1-d_f)E_{11}} & -\frac{\upsilon_{21}}{E_{11}} & 0 \\ -\frac{\upsilon_{12}}{E_{22}} & \frac{1}{(1-d_m)E_{22}} & 0 \\ 0 & 0 & \frac{1}{(1-d_s)G} \end{pmatrix}$$

Its inverse becomes: [17]

$$C_D = \frac{1}{D} \begin{pmatrix} (1-d_f)E_{11} & (1-d_f)(1-d_m)\upsilon_{21}E_{22} & 0 \\ (1-d_f)(1-d_m)\upsilon_{12}E_{11} & (1-d_m)E_{22} & 0 \\ 0 & 0 & D(1-d_s)G \end{pmatrix} \quad \textbf{Eq. 14}$$

Where $D = 1-(1-d_f)(1-d_m)\upsilon_{12}\upsilon_{21} > 0$

The stresses are now computed from equation 15.

$$\sigma = C_D \varepsilon \quad \textbf{Eq. 15}$$

Here, d_f, d_m and d_s describes current amount of damage in the fiber and matrix and contains both tension and compression damage. They are calculated from $d_f^t, d_f^c, d_m^t, d_m^c$ corresponding to the four failure modes. The way these are calculated in ABAQUS is to introduce a characteristic length (typically the length of an element) so that the constitutive law is expressed in equivalent stress vs equivalent displacement, see Figure 9. From O to A the undamaged elastic response of an element is shown, and A-C is the linear stiffness degradation. A is the point where damage is initiated for the current mode. The area under this graph is the fracture energy, G_C, which is the energy dissipated due to failure in the current mode. [10]

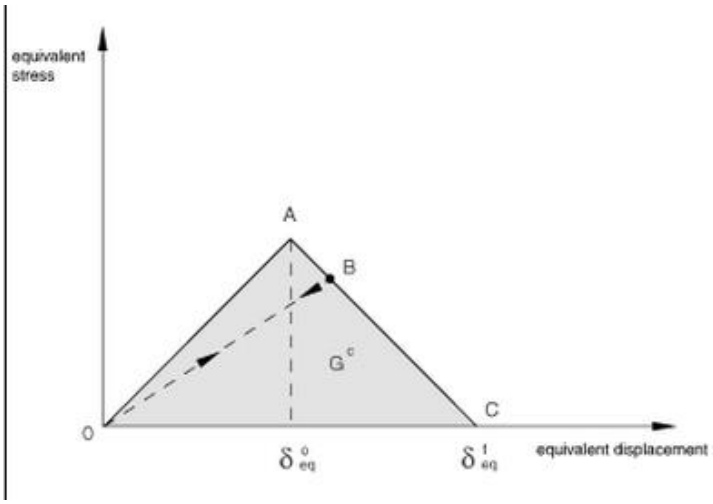

Figure 9: Equivalent stress vs equivalent displacement

When this damage model is used in ABAQUS, one has to define the longitudinal and transverse tension and compression strength. When an element is stressed to its material strength, damage is initiated to the element. The stiffness degradation or damage evolution is defined by stating the fracture energy of each mode. Estimates on the cell wall strength is found in Kettunen [7], but the fracture energies are harder to come by. The fracture energy has to be determined by laboratory tests, which is challenging given the microscopic size of a cell wall.

3 Method (Modelling in ABAQUS)

This chapter describes the modelling process of the microstructure of wood in ABAQUS. A wood block was discretized into a system of cells, where the cell walls were modelled with layered composite shell elements given the properties of the cell wall material and assigned to a grid geometry.

Two models were created, model A and model B. Model A was aimed to describe the behaviour of a wood cell system under uniform compression.

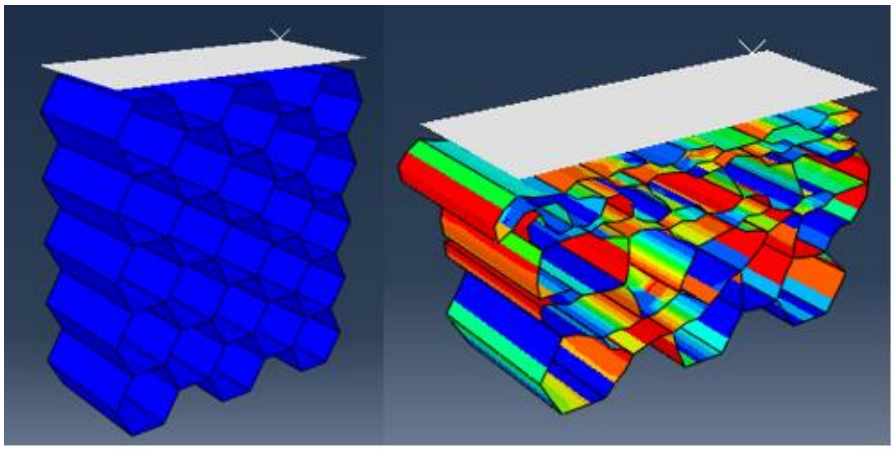

Figure 10: model A

Model B is an extended version of model A, aiming to include the effect of compressive stresses spreading out in the wood block and include the so-called hammock effect. Model B was later developed even further to contain both a shell element part and a solid element part. The shell element part was aimed to include the effect of fiber crushing under the load and the solid element part was made to describe the elastic regions of the wood. A detailed description of the models is presented in the chapters below.

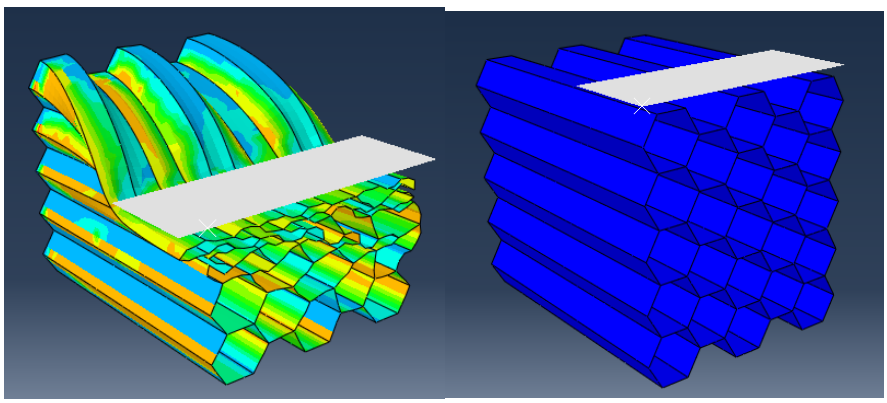

Figure 11: Model B

3.1 Consistent units

There are no built-in units in ABAQUS. The only requirement for the units is that they are consistent. Wood fibres are roughly 25-45 µm in diameter and the cell walls roughly 5 µm thick (see chapter 2.2). In addition, the forces that act on the fibres are assumed very small. The chosen system of units chosen are based on µm, µN and seconds.

	Unit
Force	**µN**
Length	**µm**
Pressure	**MPa** (µN/ µm^2)
Mass	**kg**
Density	**kg/ µm^3**
Energy	**pJ** (µN* µm= 10^{-12} N*m)
Energy/area	**N/m** **(**µN*µm/µm^2)

Table 4: Consistent units used in ABAQUS

3.2 Geometry

3.2.1 Cell walls

Recall from chapter 2.2 that the cell walls consisted of several layers where the S2 layer was the one of largest influence on total cell wall thickness. Every cell is always neighboured by another cell, which means cell walls always come in pairs. The cell walls are therefore modelled as double S2 layers glued together by a compound middle lamella (CML). In ABAQUS, this is done using a composite shell section with three layers, 2 S2 layers and one CML layer, as seen in Figure 12.

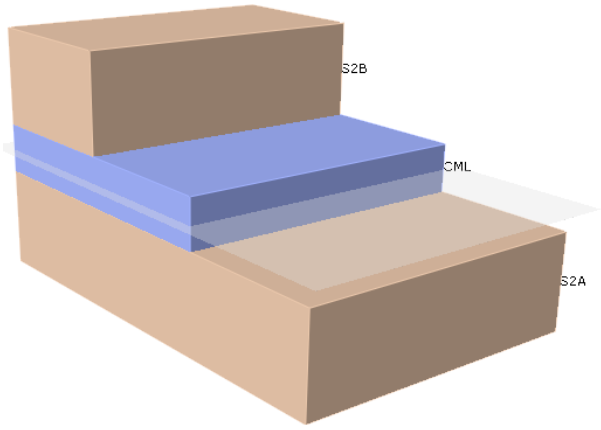

Figure 12: Ply stack plot of double cell wall in ABAQUS.

As mentioned in chapter 2.2, the thickness of the cell walls vary from 2-7 µm. To create a model of the cell walls, one value for the thickness is required, and the mean value 4.5 µm was chosen. With double cell walls, that gives a shell section with a thickness of 9 µm.

In addition, the S2 layer makes up 75% of the cell wall thickness. Since the cell wall in this model is idealized as two different layers per cell wall (S2 and CML), the shell section should consist of 75% S2 and 25% CML. The thickness of the different layers then becomes as described in figure 13.

Material	Thickness	Orientation Angle	Integration Points	Ply Name
S2	3.375	0	5	S2a
Lignin	2.25	0	3	CML
S2	3.375	0	5	S2b

Figure 13: Shell section set-up

3.2.2 Cell system

The shell section (cell wall) was assigned to a regular honeycomb grid to create the cellular structure, referred to as the cell system. A hexagon was sketched with a 15 µm radius (recall cell diameter was 20-50 µm) and mirrored to create a regular honeycomb grid.

The cross section of this hex-grid is roughly 120 µm x 130 µm (BxH). Model A was given a length (in the fibre direction) of 50 µm and model B was given a length of 150 µm.

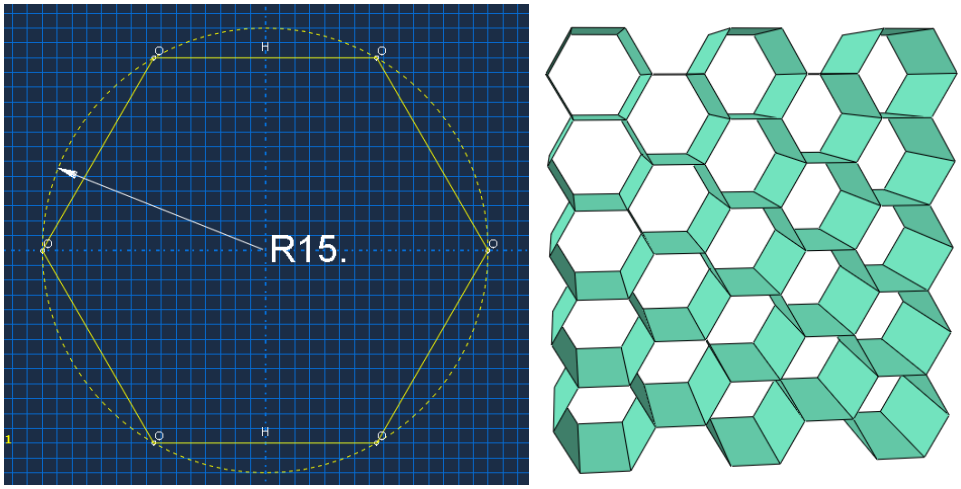

Figure: 14 Left: Single cell cross-section Right: Visualization of hex grid on model A

With this approach, every “line” in the honeycomb grid is given a double cell wall. In reality, cells that are neighboured by another cell will always have double cell walls. Cells on the edge of a wooden block will not be neighboured by other cells, so therefore the uppermost cell walls should not have double cell walls. In this model, this is only the case top layer of cells, and its effect is assumed negligible.

3.3 Material model

The cell walls were modelled with two materials, one describing the load bearing S2 layer (cellulose, hemicellulose and lignin lamina) and the other describing the compound middle lamella (lignin) acting as a binding matrix.

In addition, model B contains solid elements assigned approximate macroscopic elastic material properties of wood.

3.3.1 S2 material model

Elastic range

The S2 layer has strong directionally dependent material properties because of the cellulose microfibrils running in the length direction of the cell. It was therefore chosen to use the transversely isotropic lamina model. When defining a lamina, required input is E-modulus in the length and transverse direction, poisons ratio and shear modulus in three directions.

The exact mechanical properties of the S2 layer are not known, but we know that the cell walls gets most of its mechanical properties from the S2 layer. Kettunen [7] shows estimates on the cell wall E-modulus and yield strength in the main directions. The poisons ratio and shear moduli are harder to come by.

The E-modulus in the fibre and transverse directions are taken from chapter 2.3, and the rest of the values are assumed using engineering intuition, see table 5. In addition, the density of the S2 layer is assumed the same as the density of the cell wall. The density is 1500 kg/m^3, which in consistent units is 1.5*10^{-15} kg/**um**^{3}.

Mechanical properties of S2 material model (Lamina)	
E1 (MPa)	35000
E2 (MPa)	10000
v	0.1 (Assumption)
G12 (MPa)	5000 (Assumption)
G13 (MPa)	5000 (Assumption)
G23 (MPa)	5000 (Assumption)
Density (kg/**um**^{3})	1.5*10^{-15}

Table 5 Mechanical properties of the cell wall [7]

Non-linear range

Material non-linearity is included by assigning a Hashin damage criterion to the S2 layer. The Hashin damage model consists of a damage initiation criteria and damage evolution description.

Damage initiation

Required input for damage initiation in the Hashin damage is longitudinal and transverse tensile, compressive and shear strength. The yield strength of the cell walls is presented in table 6, but does not distinguish between compressive and tensile strength. In addition, the shear strength is unknown.

The shear strength comes into account in the matrix compression and tension damage mode, and these are the modes involved in pure transverse compression of fibres. The shear strength of the cell walls should ideally be determined by laboratory tests, but for now they are assumed equal to the yield strength in each direction.

Longitudinal tensile strength	Longitudinal compressive strength	Transverse tensile strength	Transverse compressive strength	Longitudinal shear strength	Transverse shear strength
150 MPa	150 MPa	50 MPa	50 MPa	150 Mpa	50 MPa

Table 6, Damage initiation stresses, from table 2.

Damage evolution

In the Hashin damage model, damage evolution is described by a set of fracture energies, one for each damage mode. Such fracture energies would have to be found by laboratory tests of the cell walls, but due to the microscopic size of cells, this is easier said than done. If these energies are set to zero, the element loses all its stiffness instantly when the element stress reaches the material strength. This would result in a very brittle failure model, which could work in tension where wood is known to be brittle. The goal of the numerical models created is to describe the ductile behaviour of wood in compression, therefore the fracture energies should be set to a high value. Each mode were assigned the same fracture energy, and several fracture energies were tested and results compared.

The fracture energies tested were G=0 N/m, G=1000 N/m and G=10^6 N/m. In addition, each model was tested with a linear elastic material (No Hashin damage criterion).

3.3.2 Lignin material model (CML)

Lignin is assumed isotropic and with an elastic modulus of 5.2 GPa and Poisson ratio of 0.3, taken from chapter 2.3.2.

3.3.3 Macroscopic wood material model

The elastic macroscopic properties were implemented into ABAQUS using engineering constants in the orthotropic material model. The values used are presented in table 7, but it is important to know that these are not in any way "exact" values for wood. Using "accurate" values here was not a priority, so spending time in finding "correct" would be a waste of time. The values in table 7 are loosely based on the parameters presented in chapter 2.3.3.

ρ	E_{LL}	E_{RR}	E_{TT}	G_{LR}	G_{LT}	G_{RT}	υ_{LR}	υ_{LT}	υ_{RT}
$400x10^{-18}$ kg/µm^3	10000 MPa	800 MPa	400 MPa	600 MPa	600 MPa	50 MPa	0.5	0.6	0.6

Table 7: Approximate E-moduli for wood for the macroscopic material model

3.4 Contact

The default interaction property was chosen to include the effect of cell self-contact (Normal behaviour, default constraint enforcement method). Two interactions were created, general self-contact in the cells and surface-to-surface interaction between the analytical rigid plane and the top cells.

3.5 Mesh and elements

Elements are available with reduced integration and full integration. Elements with reduced integration time are more efficient than fully integrated elements in terms of CPU time, but can produce spurious vibration modes that would have to be eliminated by some sort of hourglass control.

In all the numerical models, fully integrated elements were chosen since the analysis times were rather low. In the shell part, linear shell elements (S4) were used. In the solid part, linear solid elements (C3D8) were used.

Some sort of numerical instability occurred when trying to refine the mesh, so a coarse mesh with approximate element size of 5 µm was chosen. The element size is more thoroughly discussed in chapter 5.3.

3.6 Boundary conditions and loading

The boundary conditions of model A is presented below. In model B, the boundary conditions are similar, but they are presented in a separate chapter where model B was developed further (chapter 3.8).

3.4.1 Model A

The purpose of the model was to describe the behaviour of a few selected cells inside a larger wooden block. Thus, the boundary conditions had to ensure that the modelled cells behaved as if they were surrounded by a very large amount of cells. The boundary conditions are shown on Figure 15. The edges of the cell system (region 1) were locked in the sideways direction (x-direction) and the bottom (region 2) was given y-symmetry conditions. In addition, the model was locked in the z-direction to avoid column-type buckling in the z-direction.

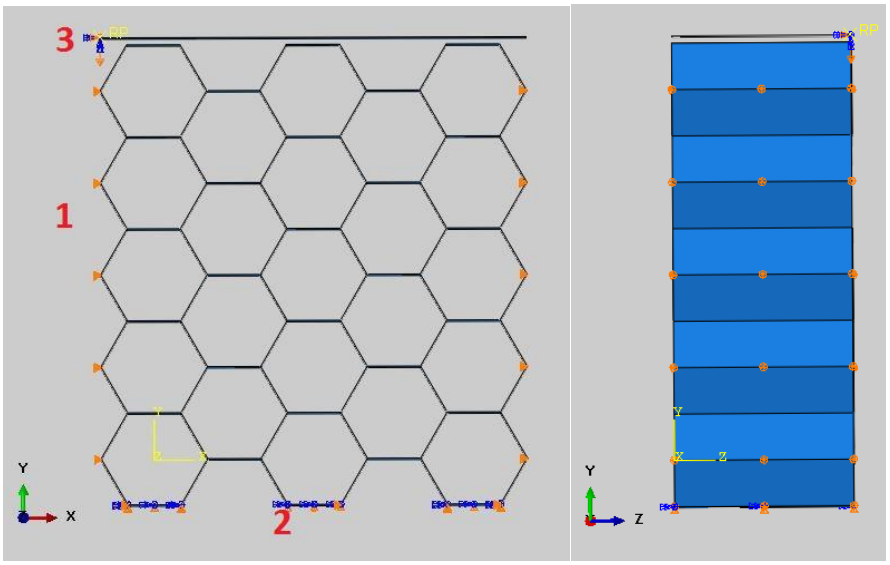

Figure 15: Boundary conditions of model A

When loading a structure, one can use either load-controlled or displacement-controlled loading. In this case, the load is unknown, making load-controlled loading difficult. In addition, load-controlled loading may lead to convergence difficulties in severely non-linear problems with material softening and buckling. It was therefore chosen to model the loading with a displacement-controlled rigid plane (region 3). The hex structure is roughly 120 µm tall, and for buckling and self-contact in the cells to happen one needs severe deformation. The rigid plane was therefore set to go down 60 µm, crushing the structure to half its original height

3.7 Analysis procedure

Initially, attempts at solving the problem with a static analysis in Abaqus/standard were carried out. Due to the large amount of buckling and material non-linearities, this approach was very sensitive to convergence difficulties. Instead, solving the model with an explicit dynamic analysis was chosen, since explicit analysis are more suited for complex contact conditions and buckling.

When modelling a quasi-static problem with explicit dynamics, one has to make sure the loading is slow enough so that inertia forces are insignificant. Recall from chapter 2.4.2 the different methods for checking the quality of the solution. The kinetic energy and viscous dissipation energy should be considerably lower than the internal energy. In addition, the total energy balance should be constant or close to constant throughout the analysis. This has to be checked for every analysis.

In ABAQUS, numerical damping is applied by default to damp out high frequency vibration ("ringing"). The default values of 0.06 for linear bulk viscosity and 1.2 for quadratic bulk viscosity was chosen.

When the analysis starts and the loading plane hits the model, kinetic energy is bound to occur since the elements starts to move. In order to decrease sudden movement when the load starts, a smooth step amplitude was applied to the prescribed displacement of the loading plane. In ABAQUS, a smooth step amplitudes applies the displacement with a fifth order polynomial, see Figure 16

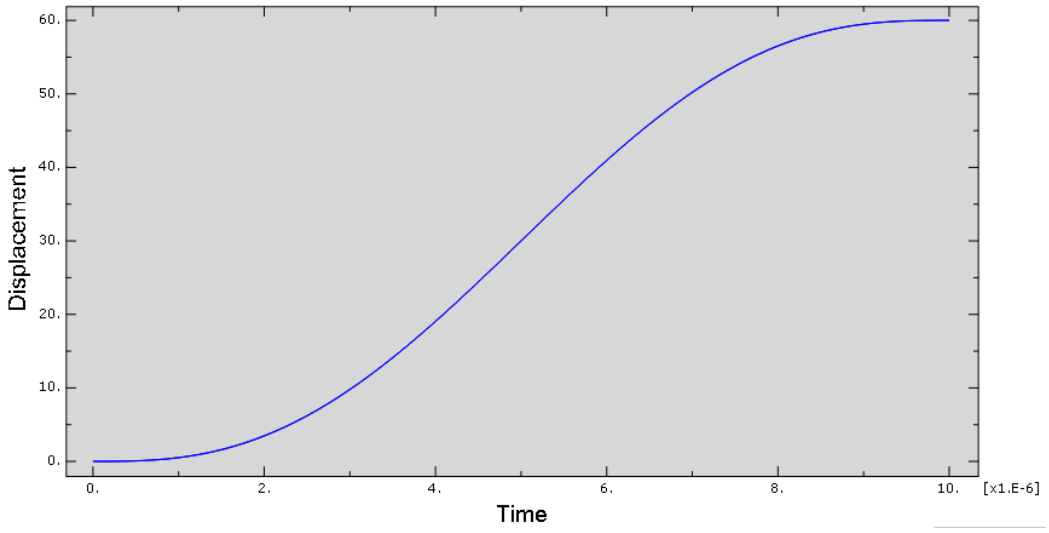

Figure 16: Displacement is applied with a fifth order polynomial

3.7.1 Loading rate and mass scaling

The models had to be given a certain time span for the loading to be applied. The time span had to be short enough to keep the analysis time low, and long enough to keep the inertia forces low. Increasing the loading rate and scaling the mass does the same thing: speeding up the analysis. For simplicity, it was chosen to only increase the loading rate and keep the mass constant.

The initial total time set was 10^{-5} seconds, since this loading rate seemed to keep the analysis time low and dynamic forces to an insignificant level. If any jobs showed signs of significant dynamic effects, the job was run again with a total time of 10^{-4} seconds.

3.8 Further development of model B

Initially, model B was an adjusted version of model A with three times longer fibres and slightly different boundary conditions. On the edge by the loading plane (right side on Figure 17), symmetry conditions were assigned. On the opposing edge (left), furthest away from the load, the rotation and translation in the fibre-direction was fixed. The edge was still free to move in the vertical direction.

Ideally, the model should be much longer, but it was assumed that the effect of a longer model would be included by fixing the left end.

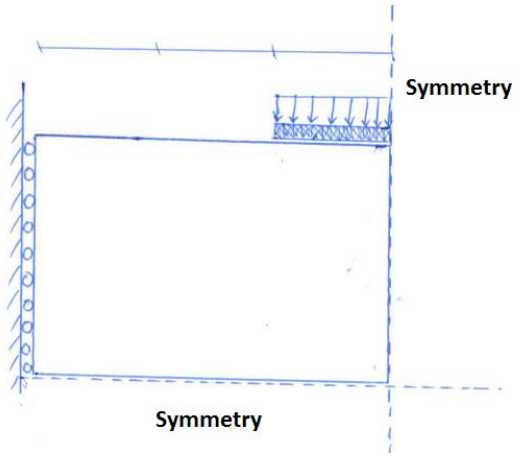

Figure 17: Initial boundary conditions of model B

Modelling each fibre with shell elements was primarily done to properly describe crushing of the wood fibres. When wood is compressed, usually the area under the load is the only place where material non-linearity occurs (if we disregard cracks). This means that if we want to model an entire wooden block subject to transverse compression, only a part of the block has to be modelled with shell elements. In the rest of the block, the material behaves linearly and can thus be described with solid elements given the macroscopic elastic properties of wood.

The main advantage with solid elements and macroscopic material properties is that they can easily be scaled up to describe the behaviour of an entire block of wood. Shell elements are limited to the size of a cell, which makes the largest possible shell element in the magnitude of micrometres. By connecting the shell part to blocks made of solid elements, fibre crushing is taken into account with the shell part and the elastic response of the rest of the block is included with the solid elements.

Building a model with both shell elements and solid elements requires some connection between shell and solid elements. In ABAQUS, this is relatively easily done by using the shell-to-solid coupling, which connects a shell edge to a solid surface.

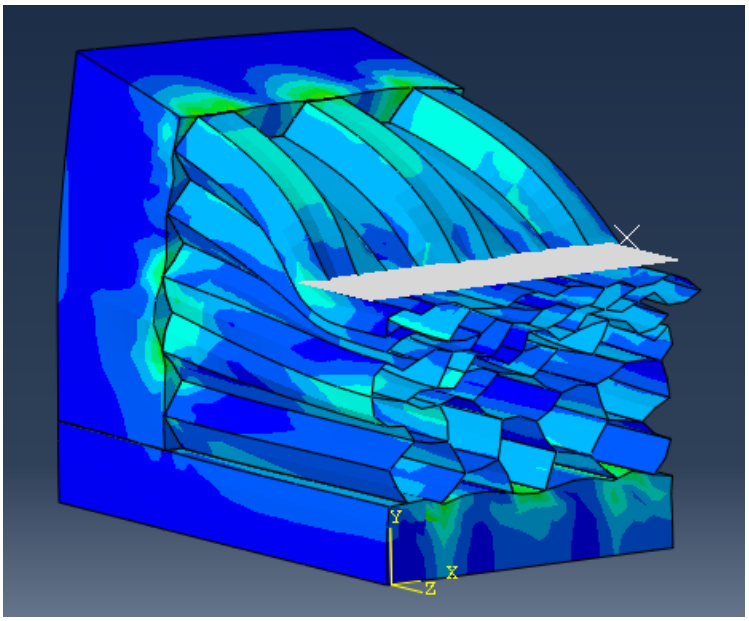

Figure 18: Model B connected to blocks of solid elements

The goal of the development of model B was not to model the entire wooden block, but to see how connecting a solid element part to the shell element part would affect the response.

Initially, in model B, translation in the length (fibre) direction was fixed in the edge opposing the load, see Figure 19. In a real wooden block, the fibres are stretched (hammock effect), and can therefore translate slightly. Allowing the fibres to translate freely would result in an overly soft system and fixing the translation would make the system too stiff. Something between the two extremes is to introduce spring stiffness to the edge, which would be the most realistic idealization.

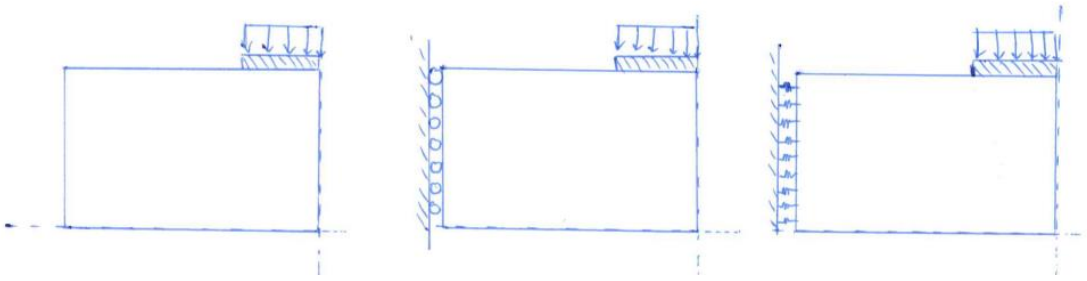

Figure 19: Left end free to translate, fixed and assigned spring stiffness.

Replacing the boundary conditions on this edge with a block made of solid elements would allow the fibres to move slightly. The spring stiffness from Figure 19 would then be dependent of the bending and shear stiffness of the block.

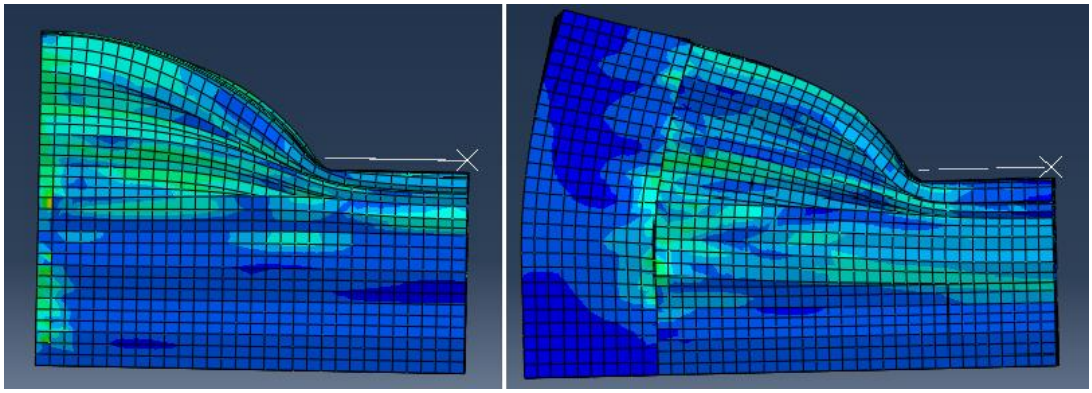

Figure 20: Left end fixed (left) and left end held back by a block of solid elements (right)

With this the first solid block attached in the fibre direction (Figure 20), the model is easily expanded in the fibre-direction. Simply by changing the length of the solid block, the model is elongated. It would be convenient to be able to expand the model in the height-direction as well, so a second solid block was attached to the underside. The blocks will from now be referred to as block 1 and block 2, see Figure 21.

To attach it to the rest of the model, block 2 had to be connected to both block 1 and the shell part. The connection between block 1 and block 2 was done using the tie-command and the connection between block 2 and the shell part was done using shell-to-solid coupling. The dimensions of the blocks were chosen just to fit the blocks to the shell part and could easily be changed.

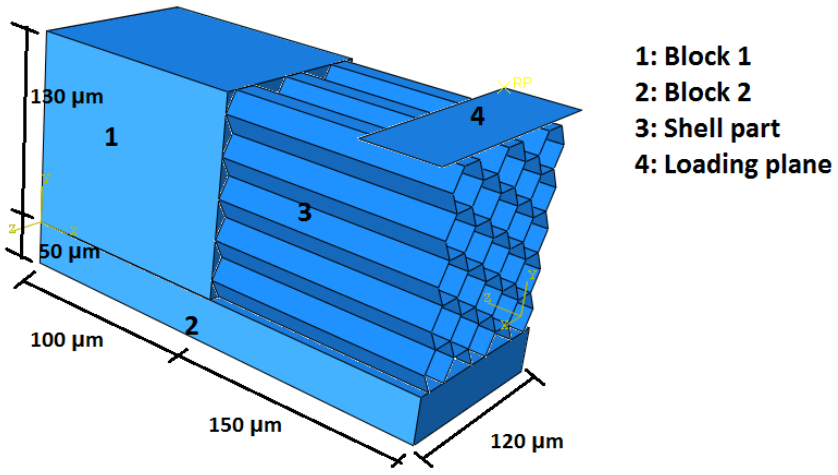

Figure 21 Overview of model B3

The solid elements were assigned the macroscopic properties taken from chapter 3.3.3. When creating an orthotropic material in ABAQUS, the material orientation has to be defined. Since the radial and tangential material properties are similar, it is assumed that the direction of these are not important. The main point is to have the same direction for the fiber properties as the shell element fibres are oriented. In ABAQUS, direction 1 is the length direction, 2 is the radial direction and 3 is the tangential direction, see Figure 22

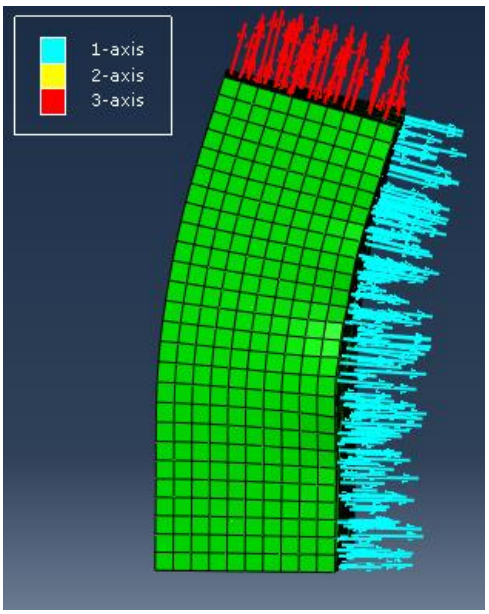

Figure 22: Material orientation of solid block in its deformed state. The 2-axis is not showin in the figure, but goes inwards.

Boundary conditions

In model A, the underside of the shell part was given y-symmetry conditions. In model B, the underside of the shell part was connected to block 2, so the boundary conditions had to be removed. The final boundary conditions on model B was z-symmetry along the edge closest to the loading, sideways locking (x-direction) of the outer cell walls and vertical movement fixed on the underside of block 2, see Figure 23.

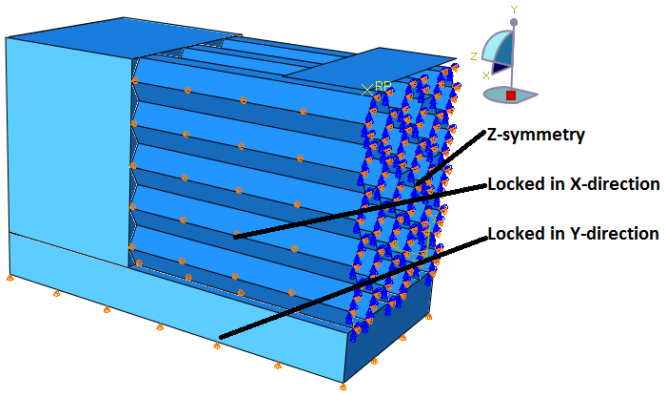

Figure 23: Boundary conditions of model B3

3.9 Summary of modelling

Two main models were created, model A and model B. Model B was developed further and attached to blocks of solid elements. To distinguish between the different versions of model B, the models were also numbered, see Figure 24.

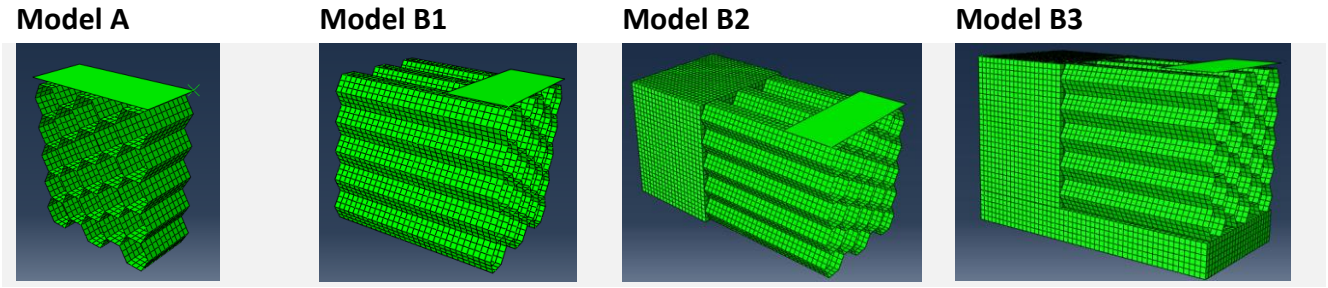

Figure 24: The four different model geometries

Two main parameters are suitable for adjustment, the cell wall thickness and the fracture energy of the cell wall. If the solution is too stiff, the cell wall thickness can be reduced to soften the system. If the solution shows brittle behaviour, the element probably loses its stiffness too fast and the fracture energy should be increased.

The energy balance must be checked in all results to ensure that dynamic forces are small compared to the static forces. The loading rate was initially set to a total time of 10^{-5} seconds. If analysis results showed signs of dynamic forces being too large to be discarded, the analysis was run again, 10 times slower.

Each of the models were tested with different fracture energies: G=0, G=10^3 and G=10^6. In addition, each model was tested without any damage criteria (linear elastic material)

4 Results

The results of the numerical simulations were given in the same consistent units as the input. In order to see the results more clearly, the *reaction force* (µN) was converted to more intuitive unit by dividing it by the area of the analytical rigid plane (6000 μm^2), to transform it into an *equivalent contact pressure* (MPa).

It is important to know that the *reaction force* is the resistance the analytical rigid plate experiences when crushing the cellular structure.

The goal of the models was to capture the effects of wood under transverse compression. The load-deformation curve of the numerical model should therefore resemble the load-deformation curve of an actual wood specimen tested in a lab (Taken from Troller's master thesis) (Figure 25).

In this chapter, the load-deformation curves of the numerical simulations are presented (Equivalent contact pressure). In addition, the energy balance is presented for each numerical simulation to show whether the dynamic effects are negligible or not. The internal energy is the sum of the strain energy and damage dissipation energy. The results are presented in here and discussed in chapter 5.

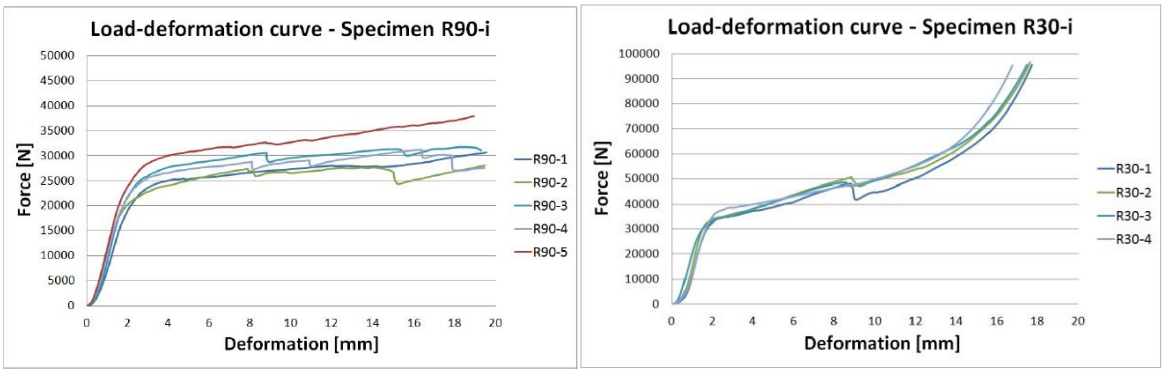

Figure 25: Load-deformation curves from Troller [12]

4.1 Equivalent contact pressure with fracture energy set to 0

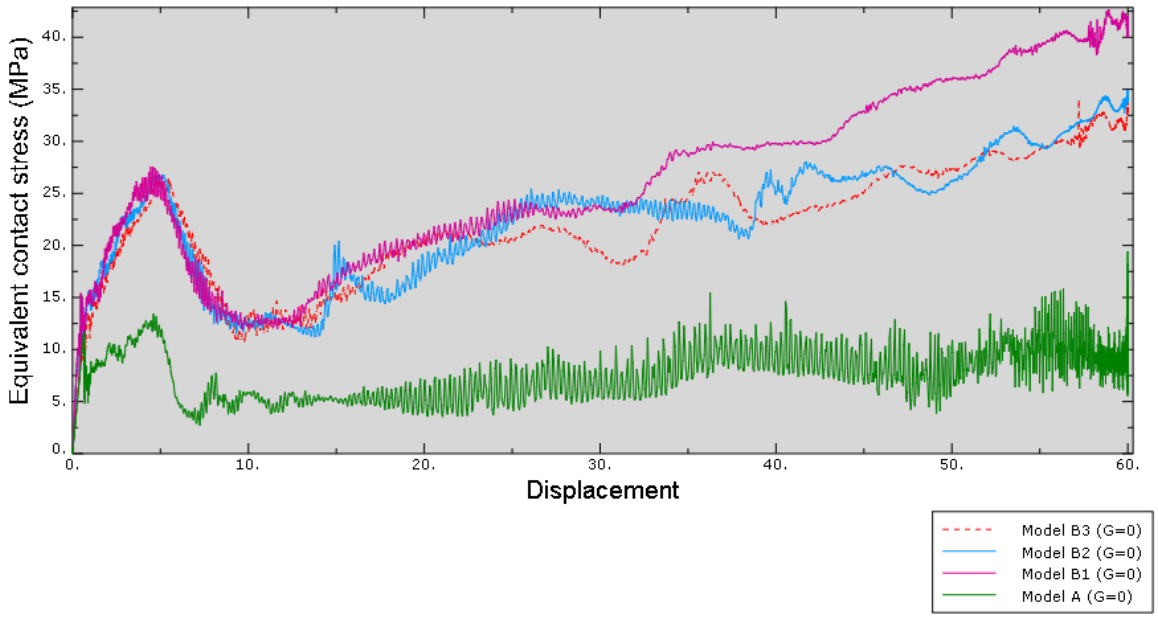

Figure 26: load-deformation curve of model A, B1, B2 and B3 with the fracture energy set to zero.

Energy balance G=0 N/m

Below, the energy balance of each model is presented. The kinetic energy is low compared to the internal energy, and the viscous dissipation is roughly 20% of the internal energy, which is too much to simply ignore.

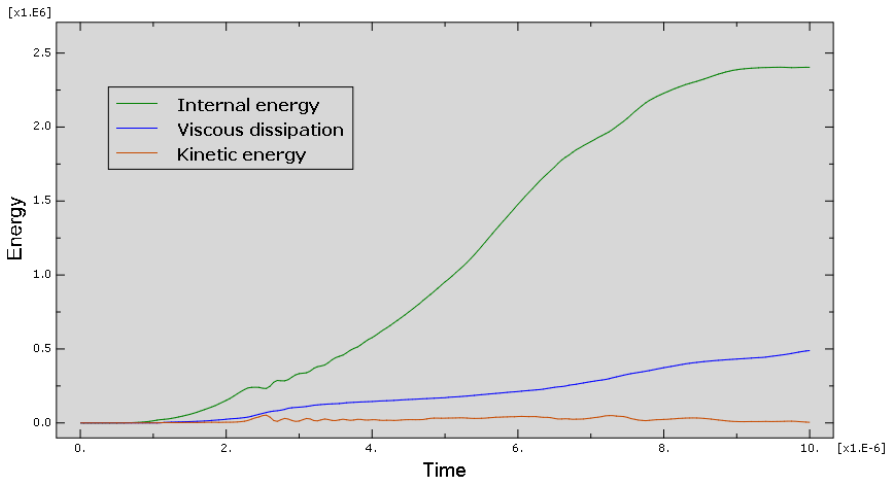

Figure 27: Model A

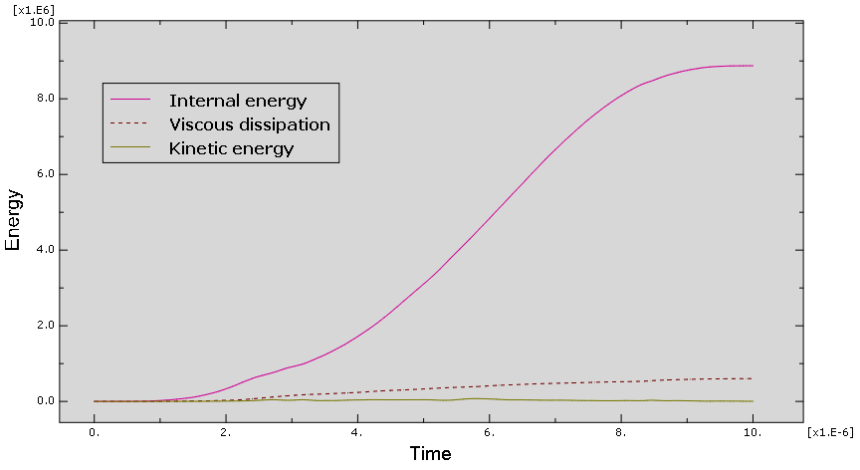

Figure 28: Model B1

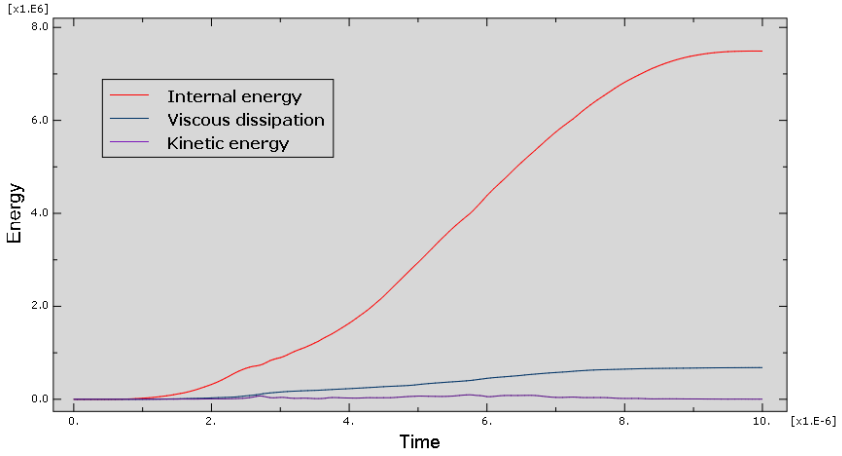

Figure 29: Model B2

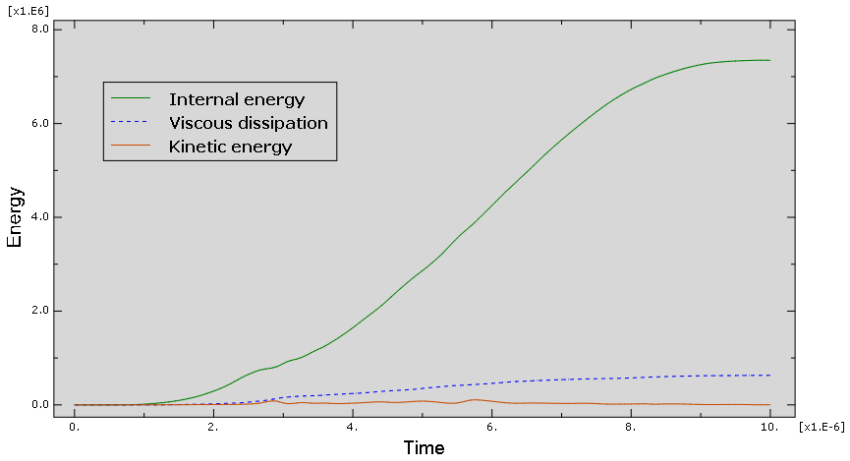

Figure 30: Model B3

4.2 Equivalent contact pressure with fracture energy set to 1000

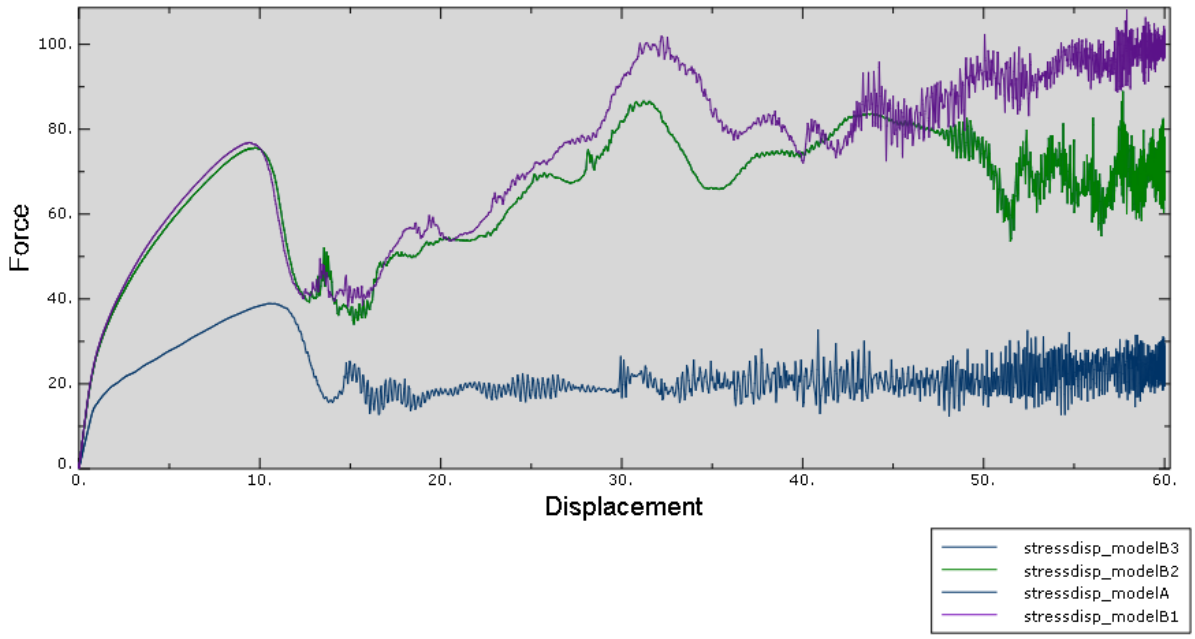

Figure 31: Load-deformation curve of model A, B1, B2 and B3 with the fracture energy set to 1000 N/m

Figure 31 shows the results of model A and model B1, B2 and B3 with fracture energy set to 1000 N/m. Model B2 and B3 have almost exactly the same load-displacement curve, which is why only three graphs are visible on the figure.

Energy balance G=1000 N/m

Below, the energy balance from the simulations with G=1000 N/m are presented. Just like the simulations with G=0 N/m, the kinetic energy is low. The viscous dissipation energy is roughly 12.5% of the internal energy, which is slightly better than the simulations with G=0 N/M

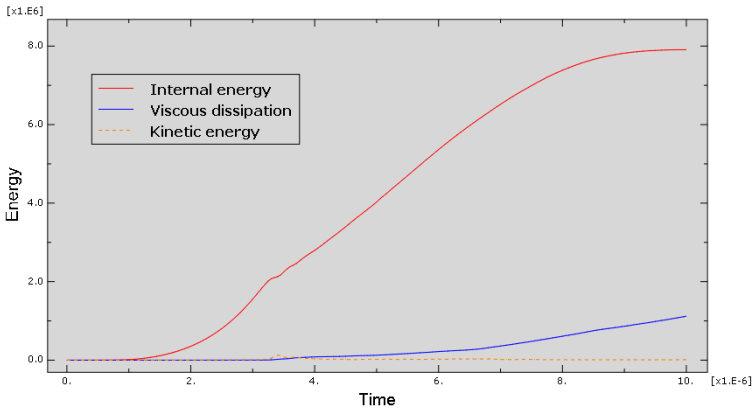

Figure 32: Model A

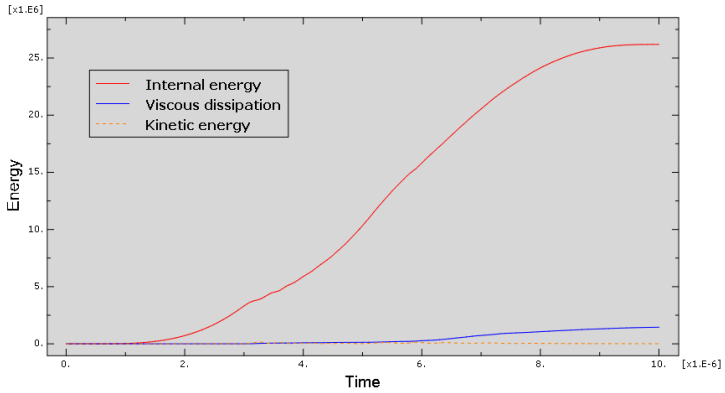

Figure 33: Model B1

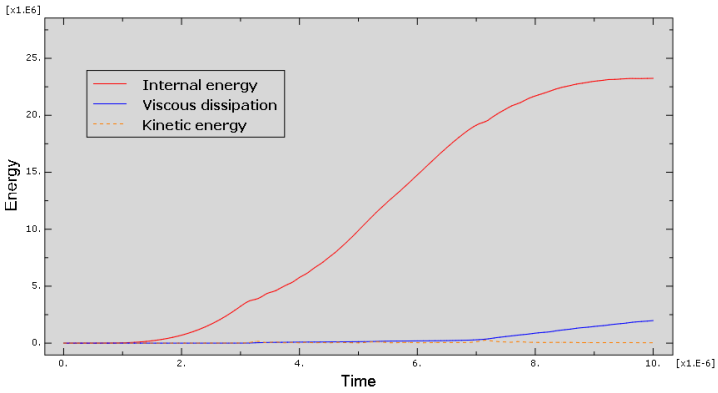

Figure 34: Modell B2

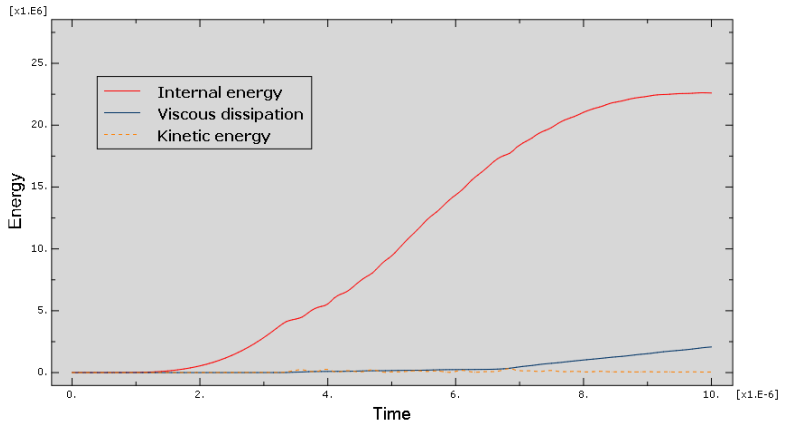

Figure 35: Model B3

4.3 Equivalent contact pressure with fracture energy set to 10^6

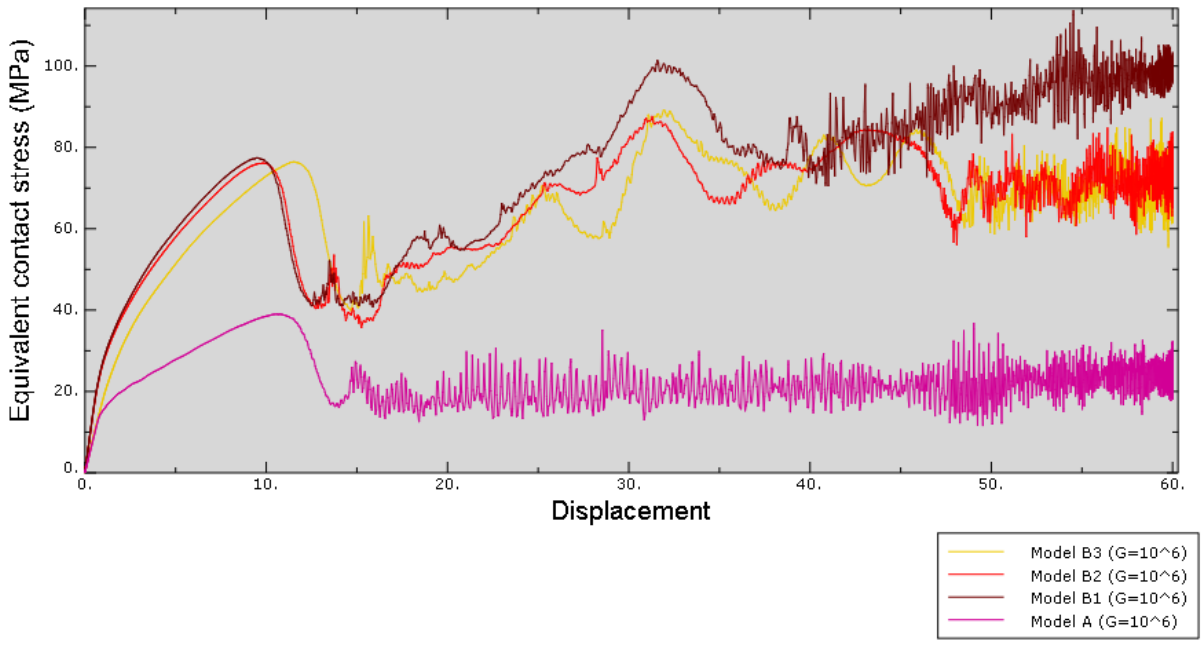

Figure 36: load-deformation curve of model A, B1, B2, B3 with the fracture energy set to zero.

Energy balance G=10^6N/m

Similar to the simulations to G=0 N/m and G=1000 N/m, the kinetic energy is low compared to the internal energy. The viscous dissipation energy is roughly the same as in the simulations with G=1000 N/m.

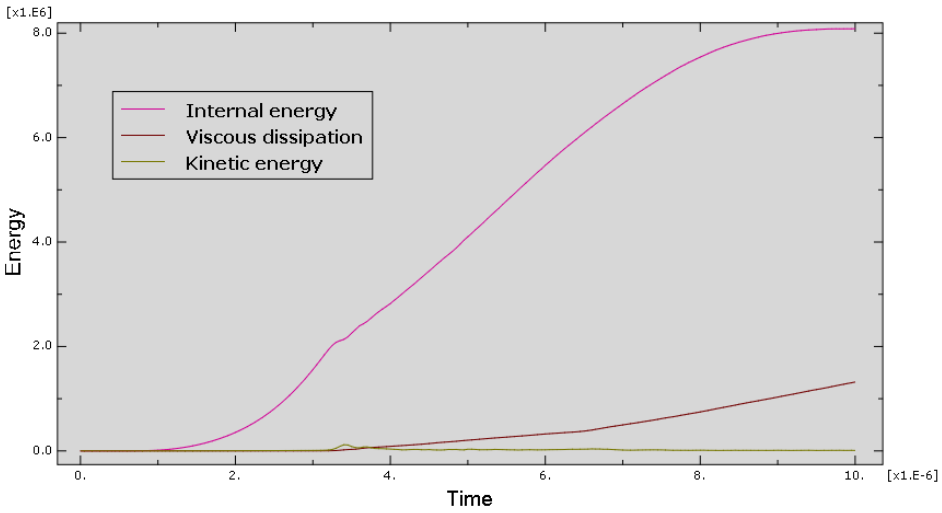

Figure 37: Model A

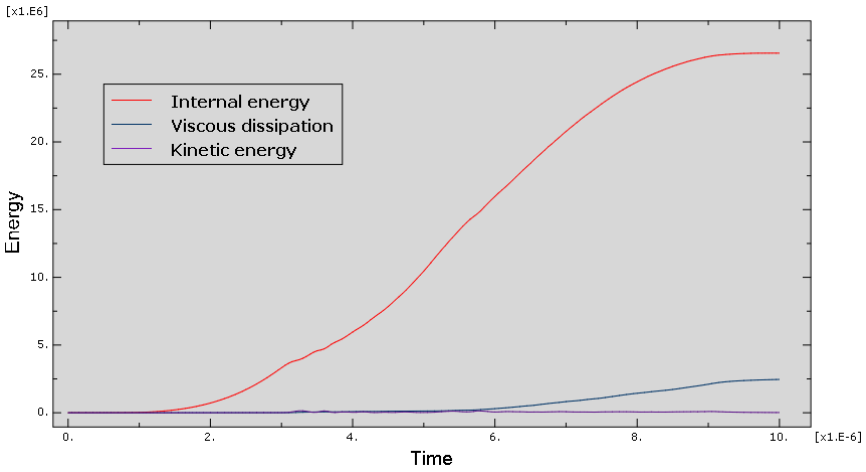

Figure 38: Model B1

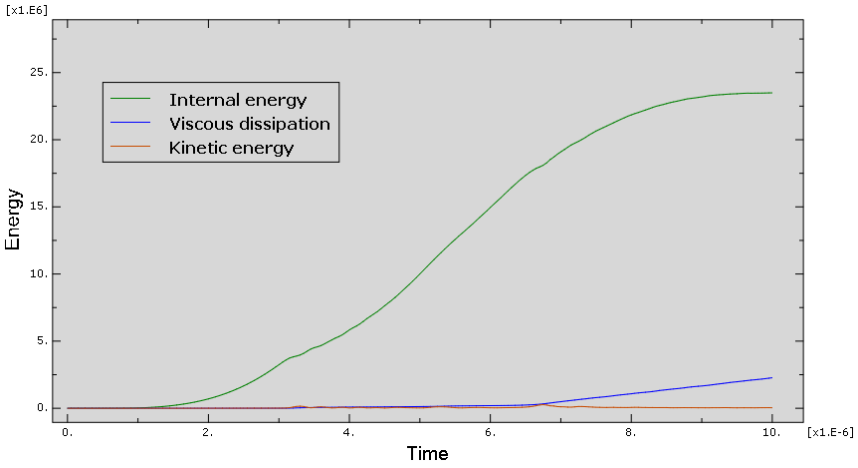

Figure 39: Model B2

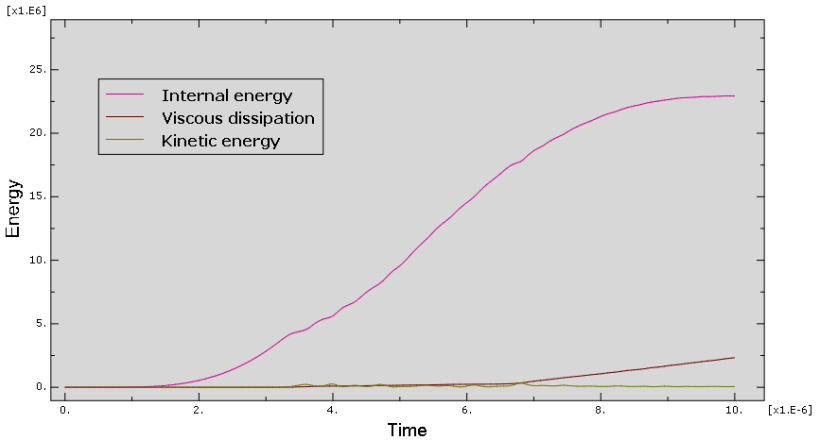

Figure 40: Model B3

4.4 Equivalent contact pressure with no damage evolution (Linear elastic material)

The models with no damage evolution were extremely stiff. The shell part did not snap like in the simulations with damage evolution. The analysis of model B3 was aborted because of excessive distortion of an element. Without damage evolution in the shells, the shell part is so much stiffer than the solid part underneath (block two), which prevents fibre crushing from occurring. In Figure 41, we see that almost all deformation takes place in the solid block, which is designed for stresses in the elastic range. No actions were made to fix this problem, since the shell section is unrealistically stiff without damage evolution.

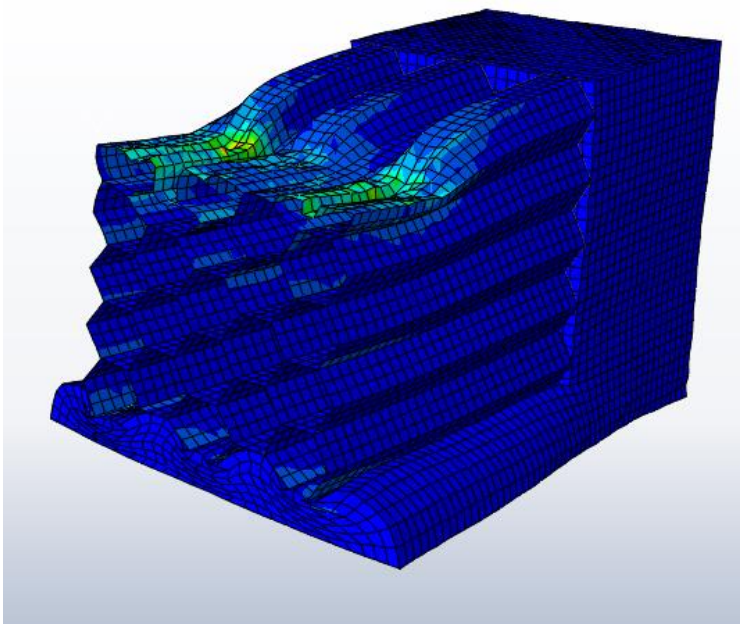

Figure 41: Overly stiff shell part causes large deformations to underlying solid block

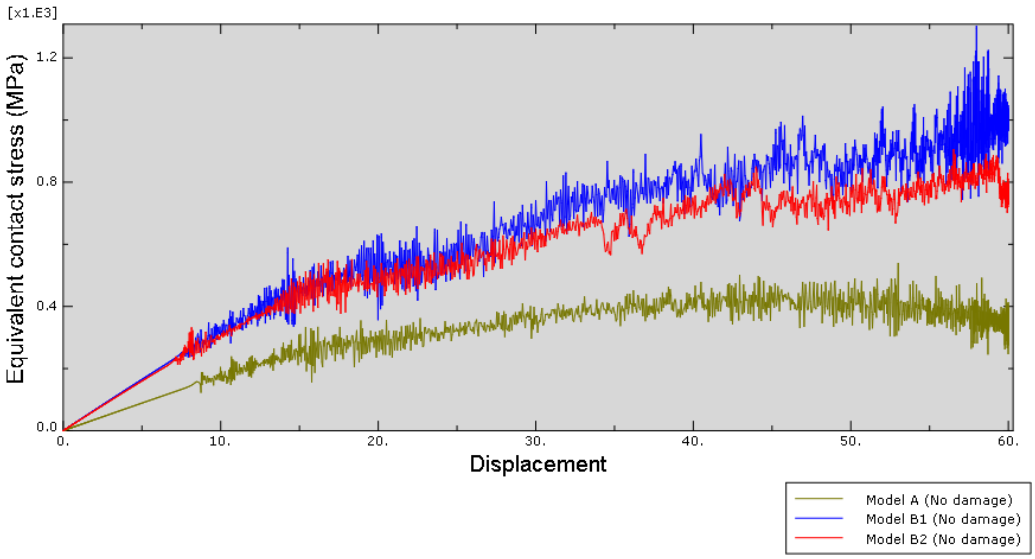

Figure 42 Equivalent pressure-displacement curve for models with linear elastic materials

Energy balance (Linear elastic material)

The kinetic energy is very low compared to the internal energy, as it should be. The viscous dissipation energy is almost twice the internal energy, which is a large error indicator. Reasons for this error is discussed in chapter 4.3.

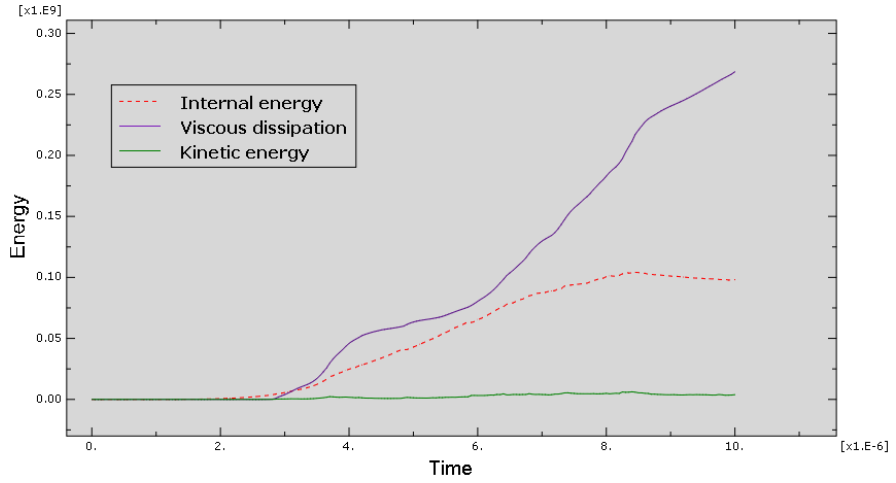

Figure 43: Model A

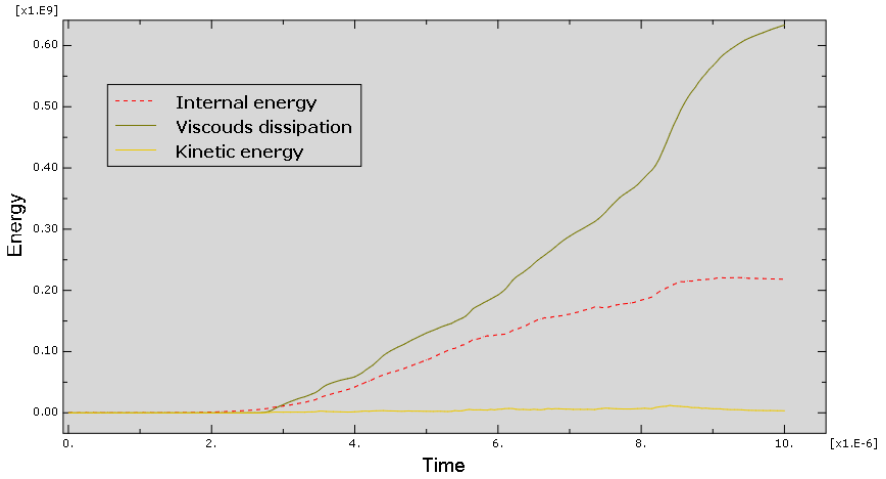

Figure 44: Model B1

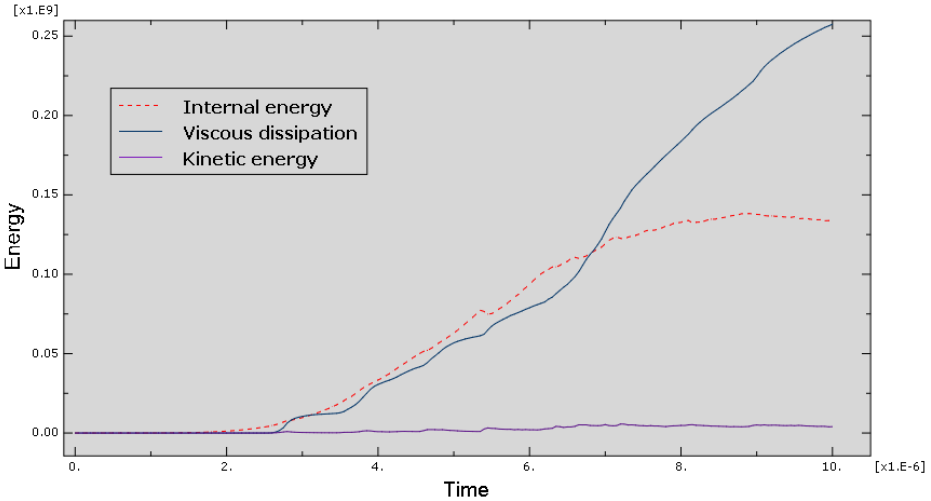

Figure 45: Model B2

5 Discussion

It is important to note that the goal of the thesis was not to produce accurate results, but rather investigate the possibilities that lie in modelling the microstructure of the wood. Therefore, the numbers are not that important, but rather the fact that that physical effects are being reproduced by the numerical models. Since getting the “correct” numbers were not a priority, the models were not calibrated to give results that are more accurate. One example of a calibration that could be made is to reduce the cell wall thickness, which would reduce the equivalent contact pressure (“reaction force”) to a more realistic value.

The load-displacement curves from the numerical results resembled to some degree those of actual lab experiment. The first part of the curve is linear, followed by strain hardening region, a stiffness drop and then further hardening. The stiffness drop is assumed to be due to a combination of material failure and buckling of the top cell layer. Self-contact later in the analysis causes the reaction force to rise, but this effect is relatively small. The effects of fibre crushing was taken into account by the buckling and contact of the cells, and the hammock effect and load distribution showed its contribution through the increase in stiffness and capacity in model B vs model A.

5.1 Cell arrangement, size and shape

In the numerical simulations carried out in this thesis, all the cells where assumed equal and placed in a regular hex grid. This is not the case for an actual wood specimen, where cell size vary greatly and the hex grid is irregular. In addition, wooden cells are not perfectly hexagonal, but of varying shapes. Some are square, circular or somewhere in between.

These cell irregularities are assumed to affect the material properties to a significant degree, but modelling the cell system quickly becomes difficult if the cell arrangement, shape and size vary. There exists algorithms that generate irregular hex grids, but not tested in this thesis.

In addition, the numerical models were limited to 25 cells. The analysis times were relatively short (15-30 min), so more cells could probably be modelled while still keeping the analysis times acceptable. The deviations between the numerical simulations and the lab results could be due to the limited number of cells and the regularity in the cell structure.

5.2 Modelling of the cell walls

The cell walls were modelled as sandwich shell sections with two S2-layers oriented parallel to the fibre direction and a compound middle lamella. In reality, the S2 layers lie with a small angle, but it is assumed that in these simulations, this angle would not affect the response. This is mainly because the angle is there to prevent cracks in the cell walls, and the numerical models in this thesis are not given crack propagation properties.

In addition, the S1 and S3 layer could have been modelled. The material properties for the S2 wall was taken from a description of the cell wall behaviour, which implies that the S1 and S3 layer is taken into account indirectly. Therefore, the S2-layer in the numerical models actually represent the entire cell wall.

5.2 Material model

The elastic properties of the cell walls is relatively well known. The uncertainties lie in non-linear part of the material model. In this thesis, Hashin damage criterion was chosen to describe the stiffness degradation and failure of the material. The Hashin damage model is designed for fiber-reinforced composites, and since the cell walls are fiber-reinforced composites, it should in theory work. However, since the fracture energy of a cell wall is unknown, it has to be assumed. If the fracture energy is set too low, the cell walls "snaps" and loses all its stiffness instantly when the yield stress is reached. If the fracture energy is set too high, the material acts almost elastic perfect plastic, with an almost horizontal stress/strain curve.

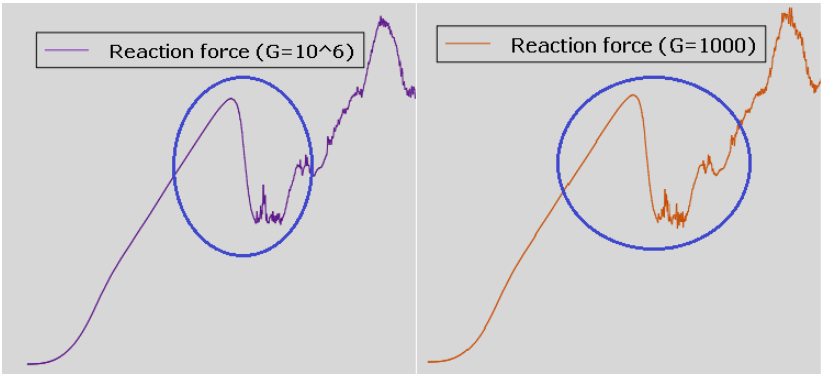

Figure 46: Sudden drop in stiffness

One of the purposes of increasing the fracture energy was to reduce the "stiffness drop" where the load-displacement curve stopped being linear, see Figure 46. However, the reaction force was almost identical for Model B1 with fracture energy set to 1000 and 10^6, as

seen in Figure 46. This could mean that this stiffness drop is due to something else than the fracture energy. Probably, it is due to one layer of cells caving in.

5.3 Numerical instabilities

When refining the mesh, the results became unrealistic. The energy balance was very different from the coarse mesh, and the external work was less than the internal energy, which is a strong error indicator. This could be due to numerical instabilities, where one element starts to spin out of control and ABAQUS has to apply large amounts of damping to slow the element down. Traces of the damping applied is seen in the energy balance in the models with no damage evolution (chapter 4.4), where the energy dissipated due to damping becomes twice the size of the internal energy. In addition, the load-deformation curve started out smooth and became spiky half way through the applied deformation.

Solutions that initially are smooth and becomes spiky points towards numerical instabilities caused by increment steps being larger than the largest stable time increment. In order to avoid this, it was attempted to reduce the increments by setting manually setting a largest allowable time increment in ABAQUS. Even with reduced increment size, the results still showed signs of numerical instability. The time increments could be reduced even more, but then the analysis would be very expensive in terms of CPU time.

This instability was very dependent on the resolution of the mesh. Very fine meshes got very large instabilities and often aborted analysis, where coarser meshes produced acceptable amounts of instabilities. In the end I chose to use the mesh that was fine enough to capture the cell geometry and coarse enough to avoid problems with the energy balance and stability.

Every simulation had to some degree spiky tendencies in the reaction force. Usually, the graphs were smooth initially but started to “vibrate” towards the end of the analysis. Presented in Figure 47 is the reaction force of model B3 with G=1000 N/m and the viscous dissipation energy. We see that the reaction force starts to become unstable at around $7*10^{-6}$ seconds and that ABAQUS applies numerical damping to stabilize the solution.

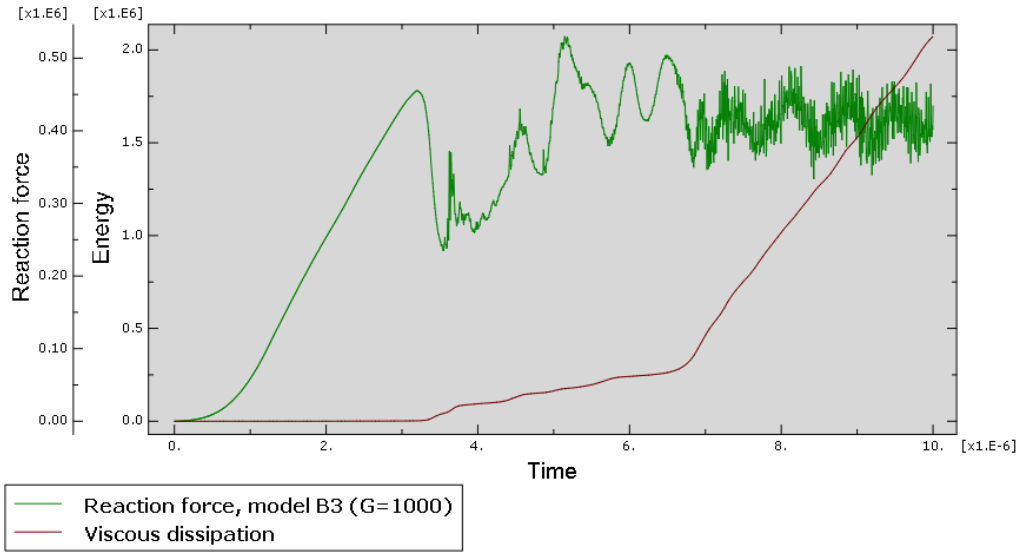

Figure 47: Reaction force and viscous dissipation energy from model B3 with G=1000 N/m

In the simulations with Hashin damage, this unstableness was still present, but to a smaller degree, as can be seen in the chapter 4. The viscous dissipated energy usually stayed under 15% of the internal energy. Ideally, the viscous dissipated energy should be even lower, but any attempts in decreasing the viscous dissipated energy has been unsuccessful.

The simulations with linear elastic material (no damage) were very unstable, producing very large amounts of viscous dissipation energy. The total energy, which should be close to constant, exceeded the internal energy by a factor of two (Figure 48). This is assumed to be due to the unrealistically large stresses in the cell walls. The normal stresses in the cell walls were between 10^4 and 10^5 MPa. The eigenfrequency of an element is dependent on the stresses in the element, and the stable time increment is dependent on the eigenfrequency. When the stresses are unrealistically large, the eigenfrequency becomes unrealistic and thus the stable time increment is changed, which is what the author believes to be the reason for the numerical instabilities.

No further attempts were made to reduce the instabilities in the simulations with linear elastic material, since the assumption of linear elastic materials in such a problem (fibre crushing, extreme displacement, self-contact, buckling) is wrong.

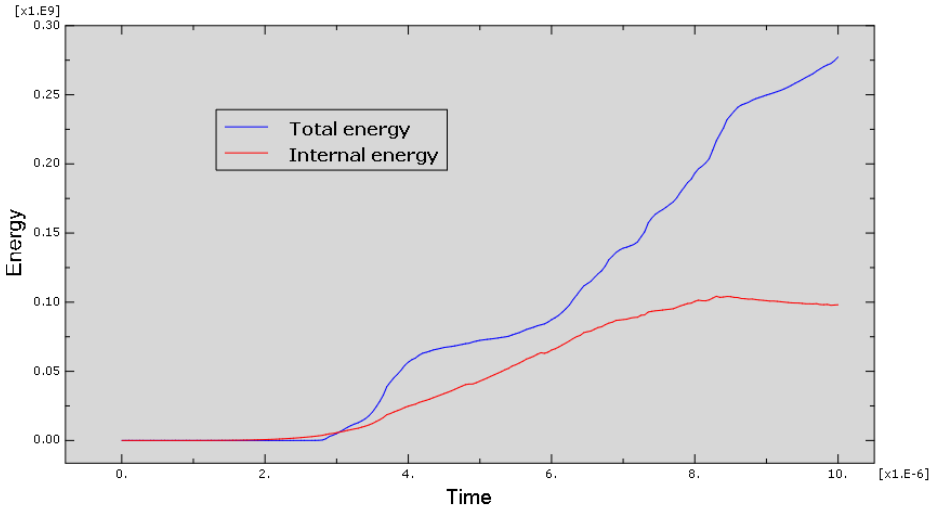

Figure 48: Total energy and internal energy in model A with linear elastic material properties.

5.4 Loading rate

In all simulations, the kinetic energy was very low compared to the internal energy. The viscous dissipation energy were a bit larger, but it is assumed that this is not due to the loading rate, but the numerical instability of the analysis mentioned in 4.3. The loading rate is therefore assumed sufficiently slow.

6 Conclusion

In this thesis, theoretical background for wood microstructure has been presented and numerical simulations to describe wood under transverse compression has been carried out in ABAQUS. Instead of modelling wood as a continuum, each fibre has been modelled separately with the microscopic material properties of a cell wall. The cells were modelled with composite shell elements describing the double cell walls where two cells meet. The main reason for modelling each cell individually was to capture the effects of buckling, collapse and self-contact of cell layers. Attempts to scale the model up to the macro scale were made. By attaching a block with solid elements given the macroscopic behaviour to the shell elements with microscopic behaviour, the model can be scaled up.

The results were plagued by some numerical instabilities due to the severe deformation of cell system, but mostly the effects of this were relatively small. The load-displacement curve of the numerical simulations resembled to some degree that of a lab experiment. With further development of microstructure modelling, the results can expected to be even closer to lab experiments.

The goal of this thesis was mainly to investigate the possibilities that lie in microstructure modelling. Judging by the results, it should be possible to create a numerical model of microstructure that accurately describes material nonlinearity and failure modes of wood. The design of joints is especially dependent on a good material model, and microstructure modelling combined with macro modelling would be a good tool for numerical analysis of joints.

7 Further work

Numerical modelling of the wood microstructure has potential for further development. When tied together with a macro model it can be a good tool to model various wood joints. The numerical models presented in this thesis needs to be developed further to more accurately capture the behaviour of wood.

Element deletion should be applied to the cell walls, so that the fibres could be “sheared off” given large enough displacement (see figure 49). This would give better failure prediction.

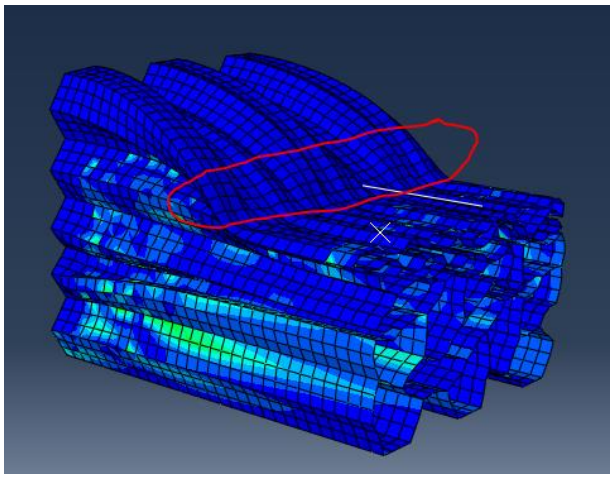

Figure 49: If the elements within the red ring were assigned an element deletion criterion, the model could be more accurate.

One effect that should be taken into account is splitting of fibres, usually present in tension perpendicular to the grain. In other work, this is accounted for by the use of extended finite element method (XFEM), so an implementation of XFEM on the microstructure could be interesting.

Because of convergence issues, the simulations in this thesis were carried out using an explicit dynamic formulation. Further attempts should be made on creating a static implicit model that converges and compare results with the dynamic results. By introducing stabilization parameters, convergence should be easier to find in ABAQUS. Other means to make an implicit model to converge under buckling is to introduce imperfections into the model. An example of an imperfection is to reduce the thickness of one cell wall in the cellular system. This would bring the model closer to reality since cell walls in an actual tree will vary.

Another improvement the model could benefit from is to introduce an irregular cell structure. In this thesis, only a regular cell structure was tested, but it would be interesting to compare results to see if changes are substantial. One way to create such an irregular cell structure is to use an algorithm based on a Voronoi diagram.

The cell walls were modelled as one binding or glue layer (CML) and one load-bearing layer on each side by using a composite shell section. It would be interesting to model all the layers in the cell wall (S1, S2, S3 and primary wall), including the microfibril angle of each layer. Then one could remove one layer and compare with the previous results to see the effects of each layer. In addition, cohesive elements could be used between the layers to allow them to slide, which could be used to predict delamination. A very thorough understanding of shell elements in ABAQUS is required of the user to do this.

In this thesis, only transverse compression of the microstructure was modelled. It would be interesting to see how microstructure modelling responds to different kind of loading. Tension perpendicular to the grain, compression and tension parallel to the grain and shear could be investigated. In addition, one could load the microstructure with oscillating loads to see if one can reproduce the internal material damping that comes from the inclination of the microfibrils in the cell walls.

The main disadvantage with modelling fibre crushing on the micro scale is the difficulties that lie in scaling it up to the macro scale. A numerical model for actual engineering application must work well on the macro scale, since fibre crushing is practically a macro scale problem in joints. More work should also be done on modelling wood on the macro scale. One idea is development a model similar to the crushable foam model that supports an orthotropic elastic material. This could be accomplished by writing a user subroutine in ABAQUS (UMAT or VUMAT).

References

1. Butterfield, B.G., B.A. Meylan, and SpringerLink, *Three-dimensional structure of wood : An Ultrastructural Approach*. 1980, Springer Netherlands: Dordrecht.
2. Record, S.J., *The Mechanical Properties of Wood Including a Discussion of the Factors Affecting the Mechanical Properties, and Methods of Timber Testing*. 2004.
3. Smith, I., E. Landis, and M. Gong, *Fracture and fatigue in wood*. 2003, Chichester: Wiley.
4. *Strength and Physical Properties of Wood*. 1981, TORONTO; BUFFALO; LONDON: TORONTO; BUFFALO; LONDON: University of Toronto Press. 71.
5. Deng, Q., S. Li, and Y. Chen, *Mechanical properties and failure mechanism of wood cell wall layers.* Comput. Mater. Sci., 2012. **62**: p. 221-226.
6. Dahl, K.B., *Mechanical properties of clear wood from Norway spruce*. 2009, Norwegian University of Science and Technology, Faculty of Engineering Science and Technology, Department of Structural Engineering: Trondheim.
7. Kettunen, P.O., *Advances in materials science of wood : special topic volume with invited papers only*. 2009, Trans Tech Publications: Stafa-Zurich, Switzerland.
8. Booker, R. and J. Sell, *The nanostructure of the cell wall of softwoods and its functions in a living tree.* Holz Als Roh-und Werkst., 1998. **56**(1): p. 1-8.
9. Picture from http://en.wikipedia.org/wiki/Pith.
10. Simulia: Abaqus Analysis User's manual (6.13)
11. Bergander, A. and L. Salmén, *Cell wall properties and their effects on the mechanical properties of fibers.* Journal of Materials Science, 2002. **37**(1): p. 151-156.
12. Troller, J., *Compression Capacity of Timber Sills Loaded Perpendicular to the Grain.* 2014.
13. Eurocode 5, Standard Norge, *Design of timber structures*, *NS-EN 1995-1-1.*
14. Bell, K., *An engineering approach to finite element analysis of linear structural mechanics problems*. 2013, Trondheim: Akademika Publ.
15. Ilstad, H. and k. Norges teknisk-naturvitenskapelige universitet Institutt for, *Validation of numerical collapse behaviour of thin-walled corrugated panels*. 1999, Department of Structural Engineering, Norwegian University of Science and Technology: Trondheim.
16. Simulia: *Quasi-static Analyses*. 2005; Available from: http://imechanica.org/files/l5-quasi-static.pdf.
17. Matzenmiller, A., J. Lubliner, and R.L. Taylor, *A constitutive model for anisotropic damage in fiber-composites.* Mechanics of Materials, 1995. **20**(2): p. 125-152.